Spin instabilities in coupled semiconductor quantum wells

R. J. Radtke,* P. I. Tamborenea,† and S. Das Sarma
Department of Physics, University of Maryland, College Park, Maryland 20742-4111
(Received 8 April 1996; revised manuscript received 26 June 1996)

We study the magnetic phases of two coupled two-dimensional electron gases in order to determine under what circumstances these phases may occur in real semiconductor quantum wells, and what the experimental properties of the broken-symmetry ground states may be. Within the local-density approximation to time-dependent density-functional theory (DFT), we find a phase transition signaled by the vanishing of the intersubband spin-density excitations at low but accessible ($\sim 10^{10}$–10^{11} cm^{-2}) electron densities. Through a self-consistent Hartree-Fock calculation, we associate this transition with an antiferromagnetic phase and study the phase diagram, thermodynamics, and collective modes in it. The collective modes are in principle observable in inelastic light-scattering experiments, and we discuss the implications of our calculations for these measurements. We also examine the ferromagnetic transition in both single and double quantum wells within the local-spin-density approximation to DFT, and obtain a critical density which depends on the well width and which is far below that of the antiferromagnetic transition. [S0163-1829(96)02844-5]

I. INTRODUCTION

The study of spin instabilities holds a fascination for both theoretical and experimental condensed-matter physicists. To theorists, these instabilities illustrate the qualitatively new states of matter which may result in simple systems through the presence of electron-electron interactions. To experimentalists, they lead to interesting phases with unique and potentially useful properties. Consequently, the search for systems which exhibit unusual spin instabilities is an area of active research, and any guidance that theory can provide which suggests avenues for this investigation should be welcome.

One class of systems ready for serious exploration are single- or double-quantum-well structures at low density. Theoretically, the low dimensionality of these structures restricts the phase space available for electron-electron scattering, increasing the relative importance of the interaction, and thereby enhancing the potential for interesting phase transitions. Another, more practical, reason for looking at these structures is that they can be physically realized in semiconductor space-charge layers and, in particular, ultrapure modulation-doped $GaAs/Al_xGa_{1-x}As$ heterostructures. These devices may be fabricated with precisely controlled dimensions that are nearly free of defects, and which are tunable over a wide range of densities and band structures. This freedom yields a large parameter space in which interesting effects may be found and explored with both experimental and theoretical tools.

In isolating the interesting regions of this parameter space, researchers can be guided by simple energetic considerations. When the kinetic energy of an electron gas dominates the Coulomb repulsion, as at high electron densities, the system behaves like a nearly ideal Fermi gas. Therefore, interesting phases will be found only in the regime in which the kinetic energy is smaller than or of the same order as the potential energy. Two ways of reaching this limit suggest themselves: applying a magnetic field or reducing the electron density. In a strong magnetic field, the kinetic energy is quenched by the Landau quantization, leading to a variety of strongly correlated quantum phases, the best-known example being the fractional quantum Hall liquid.[1–8] At extremely low densities, the electrons prefer to crystallize, as predicted some time ago by Wigner.[9] Experimental evidence of this crystallization has been somewhat equivocal in semiconductor heterostructures, but it is clearly seen in a two-dimensional electron gas suspended above the surface of liquid helium.[10] For somewhat higher densities, magnetic instabilities to spin-density wave[11] or ferromagnetic[12] phases have been proposed.

The parameter space defined by the energetics of a single low-dimensional electron gas is well defined and thoroughly explored. To find further effects, many current investigations of these systems add an additional degree of freedom by coupling two two-dimensional electron gases together. The resulting two-layer system has an additional energy scale due to the splitting of the isolated quantum-well levels into symmetric and antisymmetric components which compete with the intralayer and interlayer Coulomb energies. In a high magnetic field, this additional degree of freedom can lead to the disappearance of odd-integer and the appearance of even-integer fractional quantized Hall steps,[4,5,7] and possibly to spontaneous charge transfer between the layers.[13,14]

In zero field, a number of experimental results and theoretical predictions have also appeared in the literature.[15–25] Many of these zero-field studies focus on the behavior of the collective excitations involving transitions between the symmetric and antisymmetric levels and which are therefore unique to two-layer systems. These excitations can be produced in either the charge or spin channels, and have energies which are sensitive to the many-body interactions in the system. For example, in quantum wells with either square or parabolic confining potentials, theoretical work suggests that there exists a critical density below which the many-body corrections to the charge-density excitations cause the energy of this mode to drop below the energy of the symmetric-antisymmetric splitting.[19] This effect was recently observed by inelastic light-scattering experiments.[23] Another experimental study of coupled double-quantum-well systems re-

veals that the spin-density excitation energy abruptly merges with the continuum of intersubband single-particle excitations as the electron density is increased beyond the point at which the second-lowest subband begins to populate.[21] Time-dependent local-density approximation calculations[22] agree quite well with this experiment for most of the range of densities used, but the abrupt merge seems to demand a more refined calculation.

Of most relevance to the subject of this paper, recent calculations of the intersubband spin-density excitations in coupled double-quantum-well systems indicate that the energy of the lowest intersubband spin-density excitation may vanish at sufficiently low density.[24] The obvious interpretation of this collapse is that it indicates an electronic phase transition from the metallic Fermi-liquid phase to a condensate of zero-energy spin-density excitations. Since these excitations involve an intersubband electronic transition accompanied by a spin-flip, this condensate has been termed a spin-triplet intersubband exciton liquid. The word ''exciton'' here does not refer to the usual bound state of an electron in the conduction band and a hole in the valence band of the semiconductor; rather, it is used as a reminder that the final-state interaction or vertex correction is included in the calculation of the spin-density excitations.[26] In general terms, this transition involves the electronic spin in a fundamental way, suggesting that the ground state would have nontrivial magnetic properties. Hence the region of parameter space including the quantum-well structures exhibiting this spin-density excitation collapse are ideal candidates for the study of interesting spin instabilities.

In this paper, we examine the question of spin instabilities in such single- and double-quantum-well structures in the absence of an external magnetic field. Our goal is to determine in what structures and under what conditions these instabilities may occur, and what the experimental signatures of the ground states may be. Our primary interest is in the spin-density-excitation-collapsed phase discussed above,[24] but we also explore the more general question of ferromagnetism in single- and double-quantum-well structures. We predict that the SDE-softened phase will occur in fairly typical coupled double-quantum-well structures at low but accessible densities of order 10^{10}–10^{11} cm^{-2}, and we show that this phase corresponds to antiferromagnetic order of the spin densities in the two wells. By constructing a minimal model of the antiferromagnetic state and treating it within mean-field theory, we are able to discuss the qualitative features of this phase. In particular, we find that the transition to this state may occur at temperatures on the order of the splitting between the lowest two subbands in the quantum wells, which can be around 10 K. Moreover, although transport measurements will likely show no pronounced anomaly at the transition, both the collective excitations and the specific heat show distinctive features which can be used to identify the antiferromagnetic phase. Lowering the electron density further, our calculations indicate that these systems reenter the normal state and then enter a ferromagnetic phase at densities around 10^{9} cm^{-2}. In wide single-quantum-well structures as well, both ferromagnetic and antiferromagnetic phases exist, and we study the critical density of the ferromagnetic transition as a function of the well width. As expected from the increasing importance of exchange effects in lower dimensions, we find that the ferromagnetic phase is stable below a critical density which increases as the well width decreases.

This paper is structured in the following way. In Sec. II, we discuss the formalism which underlies our computations. In the normal and ferromagnetic states, this formalism is the density-functional theory in the local- (LDA) and local-spin-density approximations (LSDA), respectively. A time-dependent version of the LDA is also reviewed in Sec. II A, which provides quantitative results for the collective excitation spectra that we discuss in Sec. III. Additionally, in Sec. II B we describe the equations for the self-energy and the density response function in a self-consistent Hartree-Fock theory, which is the basis of our calculations within the antiferromagnetic state. In Sec. III, we reproduce and extend the results of Ref. 24, which predicted the softening of the intersubband spin-density excitations, and characterize the phase transition on the paramagnetic side in greater detail. Section IV contains a study of the ferromagnetic transition in these systems within the LSDA, and we demonstrate that that the instability predicted in Sec. III occurs at a much higher density than the ferromagnetic transition, and so cannot be associated with it. We also take a first step in the study of the ground-state spin polarization of the inhomogeneous electron gas in semiconductor quantum wells by calculating the critical density of the ferromagnetic transition in square single quantum wells as a function of well width at zero temperature. In Sec. V, we develop a simple model for the spin-density instability of Sec. III, and treat it within the self-consistent Hartree-Fock theory of Sec. II B. We study the ground state, thermodynamic quantities, and the collective-mode spectrum in the broken-symmetry phase and discuss their experimental ramifications. Section VI presents some speculations on the importance of nontrivial spin-density modulations transverse to the layering direction in these quantum-well structures, and summarizes the results of this paper.

II. FORMALISM

A. Density-functional theory

1. Unpolarized electron gas (LDA)

The central aim of this subsection is to develop the formalism used to compute the intersubband collective excitations in the unpolarized state of double and wide single quantum wells that we will use in Sec. III. We compute these collective excitations within the so-called time-dependent local-density approximation (TDLDA). This approach was first employed by Ando[27] to compute intersubband charge-density excitations (CDE's) and later extended by Katayama and Ando[28] to study resonant inelastic light scattering in semiconductor structures. The use of inelastic light scattering in these systems is motivated by the fact the charge- and the spin-density excitations (SDE's) couple to the light polarization differently, and this fact allows a selective measurement of both types of collective modes.[29,30] Detailed descriptions of the TDLDA method for calculating CDE and SDE energies and spectra have been given in the literature.[28,19] However, for the sake of completeness and to facilitate the discussion of our results in Sec. III, we describe the TDLDA

approach in some detail in the remainder of this subsection. In Sec. II A1, we shall generalize this formalism to allow for the possibility of a spin-polarized ground state of the electron gas.

The first step in the TDLDA calculation of the intersubband excitations consists of obtaining the renormalized subband energies in the local-density approximation of Refs. 31–33. We choose a coordinate system with the z axis along the direction of confinement in the quantum-well structure. The effective single-particle Schrödinger equation or Kohn-Sham equation for this system then reads

$$\left(-\frac{\hbar^2}{2m^*}\nabla^2+V_{\mathrm{EFF}}(z)\right)\Psi(\mathbf{R})=E\Psi(\mathbf{R}), \tag{1}$$

where we have assumed that the effective electron mass m^* is constant across the well, $\mathbf{R}=(\mathbf{r},z)$ denotes a three-dimensional vector, and the self-consistent effective potential $V_{\mathrm{EFF}}(z)$ is given below. The in-plane (xy) and z dependences can be separated, and, due to the assumed translational invariance in the xy plane (the localized donor charges are assumed to be smeared out uniformly in the plane), the eigenenergies and wave functions become

$$E_{n\mathbf{k}}=\varepsilon_n+\frac{\hbar^2k^2}{2m^*} \tag{2}$$

and

$$\Psi_{n\mathbf{k}}(\mathbf{R})=\frac{1}{\sqrt{A}}e^{i\mathbf{k}\cdot\mathbf{r}}\phi_n(z). \tag{3}$$

In these expressions, A is the sample area, $\mathbf{k}$ is the in-plane wave vector of the electron, and ε_n and $\phi_n(z)$ are the solutions to the one-dimensional Kohn-Sham equation

$$\left(-\frac{\hbar^2}{2m^*}\frac{d^2}{dz^2}+V_{\mathrm{EFF}}(z)\right)\phi_n(z)=\varepsilon_n\phi_n(z). \tag{4}$$

The effective single-particle potential

$$V_{\mathrm{EFF}}(z)=V_{\mathrm{CONF}}(z)+V_H(z)+V_{\mathrm{XC}}(z) \tag{5}$$

contains the confining potential of the bare quantum well $V_{\mathrm{CONF}}(z)$, and the self-consistent Hartree and exchange-correlation potentials $V_H(z)$ and $V_{\mathrm{XC}}(z)$, respectively. The Hartree potential takes into account the average electrostatic interaction with the other electrons and the positively charged donor ions, and is given by the solution of the Poisson equation

$$\frac{d^2V_H(z)}{dz^2}=-\frac{4\pi e^2}{\epsilon}[n(z)-N_D(z)], \tag{6}$$

where ϵ is the static dielectric constant of GaAs, $n(z)$ is the electron density, and $N_D(z)$ is the density of positive donor charges, which are assumed to be located far from the quantum wells. Integrating Eq. (6) twice, one obtains

$$V_H(z)=-\frac{4\pi e^2}{\epsilon}\left(\int_0^z dz'(z-z')n(z')+z\int_{-\infty}^0 dz'n(z')-\frac{N_s}{2}z\right), \tag{7}$$

where N_s is the electronic sheet density. For the exchange-correlation potential, we use the parametrization due to Ceperley and Alder[34] given by Eq. (33) in Sec. II A 2 for both the spin-polarized and -unpolarized cases.

Once the subband energies ε_n and wave functions $\phi_n(z)$ are obtained by solving Eq. (4) numerically, the z-dependent electron density is calculated from

$$n(z)=g_s\sum_{n\mathbf{k}} f(E_{n\mathbf{k}})|\Psi_{n\mathbf{k}}(\mathbf{R})|^2, \tag{8}$$

where the factor g_s accounts for the spin degeneracy and $f(E)=1/(e^{\beta E}+1)$ is the Fermi-Dirac distribution function with $\beta=1/T$ the inverse temperature ($k_B=1$ throughout this paper). This density may be rewritten as

$$n(z)=\sum_n n_n|\phi_n(z)|^2, \tag{9}$$

with the subband occupancy n_n given by

$$n_n=\frac{g_s}{A}\sum_{\mathbf{k}} f(E_{n\mathbf{k}}). \tag{10}$$

The chemical potential is determined implicitly by the relation

$$N_s=\int dzn(z)=\sum_n n_n. \tag{11}$$

At zero temperature, $f(E)\to\Theta(-E)$, and n_n becomes

$$n_n=g_sN_0(\varepsilon_F-\varepsilon_n)\Theta(\varepsilon_F-\varepsilon_n), \tag{12}$$

where Θ is the step function, ε_F is the Fermi energy, and $N_0=m^*/2\pi\hbar^2$ is the two-dimensional, single-spin density of states.

The LDA electronic structure for the spin-unpolarized case is thus obtained by solving Eq. (4) together with Eq. (7) for $V_H[n(z)]$, Eq. (33) for $V_{\mathrm{XC}}[n(z)]$, and Eq. (9) for $n(z)$ self-consistently. The results of applying this procedure to a typical double-quantum-well structure are shown in Fig. 1.

From the wave functions and eigenenergies of the LDA calculation, we can compute the collective modes of the confined electron gas which are visible in inelastic light-scattering experiments. The relation between the cross section of resonant inelastic light scattering by electronic excitations was obtained by Hamilton and McWhorter[35] for bulk systems and was adapted to the case of semiconductor heterostructures by Katayama and Ando.[28] These authors showed that the cross section for inelastic light scattering by CDE's is proportional to the imaginary part of the *reducible* electronic polarizability function $\tilde{\Pi}$ with the proportionality factors depending on the details of the band structure of the host material. These factors vanish for perpendicular polarizations of the incoming and scattered light, and are maximized for parallel polarizations. Thus CDE spectra are mea-

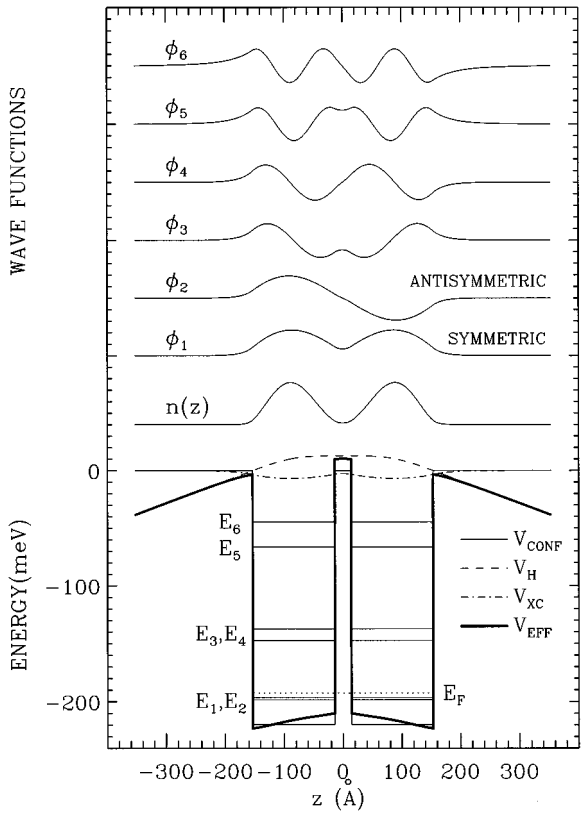

FIG. 1. Typical coupled double-quantum-well structure, and its self-consistent LDA subband energy levels E_i, eigenfunctions ϕ_i, electron density $n(z)$, and Fermi energy E_F. Also shown are the effective, Hartree, and exchange-correlation potentials $V_{\rm EFF}$, V_H, and $V_{\rm XC}$. The sheet density $N_s = 2.68\times 10^{11}$ cm^{-2}.

sured in practice within the so-called *polarized* configuration, i.e., with parallel polarizations of the two beams. On the other hand, the scattering cross section due to spin-density excitations is proportional to the imaginary part of the *irreducible* electronic polarizability function Π, which is also called the spin-polarizability function, and contains prefactors that are maximized for perpendicular polarizations of the incident and scattered beams. This is the usual geometry employed in measurements of SDE spectra, and is referred to as the *depolarized* configuration. Since we are interested in the properties of the electron gas confined in the semiconductor structure, it is sufficient to calculate the electronic response functions $\tilde{\Pi}$ and Π and ignore the band-structure-dependent factors.

We compute these response functions within the TDLDA, which is equivalent to calculating the irreducible polarizability function including a static, q-independent vertex correction in the ladder diagram approximation.[19] Within this approximation, the integral equation for the irreducible polarizability $\Pi(q,\omega)$ can be solved exactly, and gives

$$\Pi(q,\omega)=\frac{\Pi^0(q,\omega)}{1+U_{\rm XC}\Pi^0(q,\omega)}, \tag{13}$$

where $\Pi^0(q,\omega)$ is the leading-order polarizability function and $U_{\rm XC}$ is the static, q-independent vertex function. From Dyson's equation for the effective Coulomb interaction,[36] one obtains the reducible polarizability function

$$\tilde{\Pi}(q,\omega)=\frac{\Pi(q,\omega)}{1-U_H(q)\Pi(q,\omega)}, \tag{14}$$

where $U_H(q)$ is the Fourier transform of the bare Coulomb interaction. Combining Eqs. (13) and (14), we obtain

$$\tilde{\Pi}(q,\omega)=\frac{\Pi^0(q,\omega)}{1-(U_H(q)-U_{\rm XC})\Pi^0(q,\omega)}. \tag{15}$$

In a confined electron gas system, where the confinement discretizes the single-particle energy levels, the collective excitations must be calculated within a generalized dielectric function formalism.[37] In this context, the functions $U_{\rm XC}$ and $U_H(q)$ are replaced by matrices with indices labeling the different subbands. Within the TDLDA, we have

$$U^{\rm XC}_{ij,mn}=-\int dz\int dz'\,\phi_i(z)\phi_j(z)\frac{\partial V_{\rm XC}}{\partial n}(z) \times\delta(z-z')\phi_m(z')\phi_n(z') \tag{16}$$

and

$$U^{H}_{ij,mn}(q)=\frac{2\pi e^2}{\epsilon q}\int dz\,dz'\,\phi_i(z)\phi_j(z) \times e^{-q|z-z'|}\phi_m(z')\phi_n(z'), \tag{17}$$

where ϵ is the background dielectric constant.

The reducible polarizability function $\tilde{\Pi}(\mathbf{q},q_z,\omega)$, whose imaginary part is proportional to the spectrum of the CDE's and to the Raman intensity in the polarized configuration, is given by[38]

$$\tilde{\Pi}(\mathbf{q},q_z,\omega)=\int dz\int dz'\,e^{-iq_z(z-z')}\tilde{\Pi}(z,z';\mathbf{q},\omega), \tag{18}$$

with

$$\tilde{\Pi}(z,z';\mathbf{q},\omega)=\sum_{i,j,k,l}\phi_i(z)\phi_j(z)\tilde{\Pi}_{ij,kl}(\mathbf{q},\omega)\phi_k(z')\phi_l(z'), \tag{19}$$

$$\tilde{\Pi}_{ij,kl}(\mathbf{q},\omega)=\Pi^0_{ij}(\mathbf{q},\omega)\delta_{ik}\delta_{jl} +\sum_{m,n}\Pi^0_{ij}(\mathbf{q},\omega)U_{ij,mn}(q)\tilde{\Pi}_{mn,kl}(\mathbf{q},\omega), \tag{20}$$

$$U_{ij,mn}(\mathbf{q})=U^H_{ij,mn}(\mathbf{q})-U^{\rm XC}_{ij,mn}, \tag{21}$$

and

$$\Pi^0_{ij}(\mathbf{q},\omega)=2\sum_{\mathbf{k}}\frac{f(E_j(\mathbf{k}+\mathbf{q}))-f(E_i(\mathbf{k}))}{(E_j(\mathbf{k}+\mathbf{q}))-(E_i(\mathbf{k}))-\hbar(\omega+i\gamma)}. \tag{22}$$

In these equations, subscripts are the subband indices, $\mathbf{q}$ and $\mathbf{k}$ are two-dimensional in-plane wave vectors, and ϕ_j and ε_j are the LDA-calculated subband wave functions and energies. In addition, Π^0_{ij} is the leading-order polarizability function for the transition $i\rightarrow j$, $E_j(\mathbf{k})=\varepsilon_j+(\hbar^2k^2/2m^*)$, $f(E)$ is the Fermi factor, and γ is a phenomenological in-

verse scattering time; at $T=0$, an analytic expression for Π^0_{ij} can be found in Ref. 38. We note that the random-phase approximation (RPA) is obtained in the subband representation by removing the vertex correction $U^{\rm XC}_{ij,mn}$ in Eq. (21).

The imaginary part of the irreducible polarizability function Π is proportional to the SDE spectrum and to the Raman-scattering intensity in the depolarized configuration. In the subband representation, the calculation of Π is analogous to that of $\tilde{\Pi}$ [Eqs. (17)–(22)] with the following two modifications. Since the irreducible polarizability does not include dynamic Coulomb screening (spin-density excitations are unscreened by the spin-conserving Coulomb interaction), we set $U^H_{ij,mn}=0$ in Eq. (21). The second change concerns the vertex correction $U^{\rm XC}_{ij,mn}$ which for spin-density excitations is given in the TDLDA by

$$U^{\rm XC}_{ij,mn}=-\int dz\int dz'\,\phi_i(z)\phi_j(z)\frac{\partial V_{\rm XC}}{\partial m}(z) \times\delta(z-z')\phi_m(z')\phi_n(z') \tag{23}$$

instead of by Eq. (16). In this equation, $m(z)=n_\uparrow(z)-n_\downarrow(z)$ is the local spin density, $n_\uparrow$ and $n_\downarrow$ being the spin-up and spin-down local densities, respectively.

The CDE and SDE energies are given by the poles of $\tilde{\Pi}$ and Π, respectively, which occur when the determinant $|\Pi^0_{ij}U_{ij,mn}-\delta_{ij,mn}|$ vanishes. In the numerical work presented in this paper, we solve this equation keeping all the subband levels. If, as in the quantum-well structures we consider, the lowest two subbands are well separated in energy from the higher subbands, then one can approximate this determinental equation in the limit of low densities and temperatures by keeping only subbands 1 and 2, yielding

$$(\Pi^0_{12}+\Pi^0_{21})U_{12,12}=1. \tag{24}$$

For $q\to 0$, this condition gives the resonance energies in the familiar form of Ando:[27]

$$\hbar^2\tilde{\omega}^2_{21}=\varepsilon^2_{21}+2\varepsilon_{21}U_{12,12}(N_1-N_2), \tag{25}$$

where $\varepsilon_{21}\equiv\varepsilon_2-\varepsilon_1$ and $U_{12,12}=U^H_{12,12}(0)-U^{\rm XC}_{12,12}$ in the case of the CDE, and $U_{12,12}=-U^{\rm XC}_{12,12}$ for the SDEs.

2. Polarized electron gas (LSDA)

In this subsection, we introduce a generalization of the local-density approximation to density-functional theory discussed in Sec. II A 1 which allows for different populations of the two spin orientations, i.e., a finite spin polarization. This local-spin-density approximation (LSDA) formalism is also based on the self-consistent solution of the Schrödinger-like Kohn-Sham equation, coupled with the Poisson equation and a local exchange-correlation potential. The main technical difference between LSDA and LDA is that the effective exchange-correlation potential in LSDA depends on the local spin polarization as well as the electron density. Therefore, one has to solve two Kohn-Sham equations, which contain spin-dependent effective potentials, for the two components of the spinor wave function. The LSDA was first formally justified by von Barth and Hedin[39] and Pant and Rajagopal[40] and is suitable for studying ferromagnetic systems either with or without an external magnetic field.[41]

To put the LSDA approach in context, we briefly review the theoretical and numerical evidence that the uniform electron gas in two and three dimensions embedded in a uniform positive background (the jellium model) undergoes a ferromagnetic transition at a certain critical density. A simple theoretical estimate for the density at which a ferromagnetic state will form may be obtained from Hartree-Fock theory, which treats the electron-electron Coulomb interaction to first order. For a uniform electron gas in three dimensions with N_+ spin-up and N_- spin-down electrons, the ground-state energy in this approximation can be written in terms of the total number of particles $N=N_++N_-$ and the magnetization $m=(N_+-N_-)/N$ as[36]

$$E^{\rm 3D}_{\rm HF}=\frac{Ne^2}{2a_0}\frac{3}{10}\left(\frac{9\pi}{2}\right)^{2/3}\frac{1}{r_s^2}\left[\left(\frac{1+m}{2}\right)^{5/3}+\left(\frac{1-m}{2}\right)^{5/3}\right] -\frac{Ne^2}{2a_0}\frac{3}{4\pi}\left(\frac{9\pi}{2}\right)^{2/3}\frac{1}{r_s}\left[\left(\frac{1+m}{2}\right)^{4/3}+\left(\frac{1-m}{2}\right)^{4/3}\right], \tag{26}$$

where $a_0=\hbar^2/m^*e^2$ is the Bohr radius and $r_s=(3V/4\pi N)^{1/3}/a_0$ parameterizes the density. The first term in this expression is the kinetic energy, which prefers the paramagnetic state, while the second term is the exchange energy, which prefers to polarize the spins. At densities satisfying $r_s>5.45$, the exchange energy dominates, and the ferromagnetic state is stable. In two dimensions, a similar analysis yields[42]

$$E^{\rm 2D}_{\rm HF}=\frac{Ne^2}{2a_0}\left\{\frac{1+m^2}{r_s^2}-\frac{4\sqrt{2}}{3\pi r_s}[(1+m)^{3/2}+(1-m)^{3/2}]\right\}, \tag{27}$$

where now $r_s\equiv(A/\pi N)^{1/2}/a_0$. In this case, the condition for a polarized ground state, $E^{\rm 2D}_{\rm HF}(r_s,m=1)<E^{\rm 2D}_{\rm HF}(r_s,m=0)$, is satisfied if $r_s>2.01$. Thus, within the Hartree-Fock approximation, the spin-polarized state occurs at higher density (lower r_s) than in three dimensions.

Hartree-Fock theory neglects contributions to the energy beyond the exchange term, and is therefore expected to overestimate the density at which the ferromagnetic transition occurs. Including these so-called correlation terms can only be done approximately, however. Currently, the most accurate method for performing these calculations are numerically intensive Monte Carlo techniques. Ceperley and Alder[34] calculated the ground-state energy of an electron gas in two and three dimensions employing the variational Monte Carlo (VMC). They found that in both two and three dimensions there is an intermediate density regime where a fully polarized state has the lowest energy compared to the unpolarized quantum liquid and the Wigner crystal. In three dimensional (3D) the polarized phase is stable for $26<r_s<67$, and, in 2D, for $13<r_s<33$. Additional results seem to indicate that in 3D there is a transition to a partially polarized liquid at $r_s\approx 20$ and to a fully polarized phase at $r_s\approx 50$.[43] Eleven years later, Tanatar and Ceperley[44] recalculated the ground-state properties of the electron gas in two dimensions employing the VMC technique and the more accurate fixed-node Green's-function Monte Carlo (GFMC) technique. The VMC technique predicted again a transition

from the unpolarized to the polarized liquid at r_s between 10 and 20, consistent with Ceperley's results. The more accurate GFMC technique predicted a transition from the unpolarized liquid to the Wigner crystal at $r_s=37$, without an intermediate polarized phase. However, the authors point out that, near the transition, the polarized phase has an energy very close to the energy of the other phases and that, due to finite-size effects and errors associated with their approximation method, their conclusion should not be taken as definite. This leaves open the possibility of a stable, fully polarized phase in the two-dimensional electron gas.

The LSDA falls somewhere between elementary Hartree-Fock theory and Monte Carlo calculations in terms of the quantitative accuracy of its predictions. Its main strength, and the reason we use this technique here, is that it can describe the inhomogeneous electron gas which exists inside quantum-well structures and can therefore provide estimates of the critical density of the ferromagnetic transitions in these structures that could guide future experiments. In addition, the LSDA is a direct extension of the LDA, and so allows a comparison between the two calculations which will be important in ruling out ferromagnetism as the source of the spin-density-excitation softening which appears in our TDLDA calculations [cf. Sec. III]. We note that a similar problem to that of the spin polarization of the ground-state in quantum wells is the problem of ''valley condensation'' in Si-SiO_2 systems, where, instead of spin states, the electrons can occupy different valleys of the Brillouin zone. This problem has been studied in the past with techniques similar to the ones employed here.[45] In addition, the LSDA has been employed to study spin effects in wide parabolic quantum wells in the presence of a perpendicular magnetic field.[46]

Our computations in the LSDA proceed as follows. After factorizing the complete single-electron wave function as was done in Eq. (3), we write down the z-dependent Kohn-Sham equation

$$\left(-\frac{\hbar^2}{2m^*}\frac{d^2}{dz^2}+V_C(z)+V_H(z)+V_{\rm XC}^{\sigma}(z)\right)\phi_n^{\sigma}(z)=\varepsilon_n^{\sigma}\phi_n^{\sigma}(z), \tag{28}$$

where n is the subband index and σ denotes the spin orientation, which can be up (+) or down (-). We assume that no more than two subbands are populated and let $n=1$ denote the lower-energy symmetric level (S) and $n=2$ the higher-energy antisymmetric level (AS). We therefore need to consider four wave functions (ϕ_1^+, ϕ_1^-, ϕ_2^+, ϕ_2^-) and their corresponding energies in Eq. (28).

This equation also contains the exchange-correlation potential, which in the LSDA formalism depends on both the density $n(z)$ and the spin polarization $m(z)$, which is defined as

$$m(z)\equiv\frac{n_1^+(z)+n_2^+(z)-n_1^-(z)-n_2^-(z)}{n(z)}. \tag{29}$$

In our calculations, we use the parametrization of the exchange-correlation energy for the uniform 3D electron gas obtained by Ceperley and Alder,[34]

$$\epsilon_{\rm XC}^i=\frac{c^i}{r_s}+\frac{\gamma^i}{1+\beta_1^i\sqrt{r_s}+\beta_2^i r_s}, \tag{30}$$

where $i=U$ (unpolarized, $m=0$) or $i=P$ (polarized, $m=1$). The exchange-correlation contribution to the chemical potential is

$$V_{\rm XC}^i=\left(1-\frac{r_s}{3}\frac{d}{dr_s}\right)\epsilon_{\rm XC}^i=\frac{d^i}{r_s}+\gamma^i\frac{1+\frac{7}{6}\beta_1^i\sqrt{r_s}+\frac{4}{3}\beta_2^i r_s}{(1+\beta_1^i\sqrt{r_s}+\beta_2^i r_s)^2}. \tag{31}$$

The parameters in the previous expressions, as obtained by Ceperley and Alder,[34] are $c^U=-0.9163$, $c^P=-1.1540$, $d^U=-1.2218$, $d^P=-1.5393$, $\gamma^U=-0.1423$, $\gamma^P=-0.0843$, $\beta_1^U=1.0529$, $\beta_1^P=1.3981$, $\beta_2^U=0.3334$, and $\beta_2^P=0.2611$. For intermediate polarizations ($0<m<1$), we use an interpolation formula proposed by von Barth and Hedin,[39] in which the correlation energy has the same polarization dependence as the exchange energy:

$$\epsilon_{\rm XC}(r_s,m)=\epsilon_{\rm XC}^U(r_s)+f(m)(\epsilon_{\rm XC}^P(r_s)-\epsilon_{\rm XC}^U(r_s)) \tag{32}$$

and

$$V_{\rm XC}^{\sigma}(r_s,m)=V_{\rm XC}^U(r_s)+f(m)(V_{\rm XC}^P(r_s)-V_{\rm XC}^U(r_s))+(\epsilon_{\rm XC}^P(r_s)-\epsilon_{\rm XC}^U(r_s))({\rm sgn}(\sigma)-m)\frac{df}{dm}, \tag{33}$$

where

$$f(m)=\frac{(1+m)^{4/3}+(1-m)^{4/3}-2}{2^{4/3}-2}. \tag{34}$$

The Hartree potential $V_H(z)$ is calculated as in the unpolarized formalism described in Sec. II A; it satisfies Poisson equation, Eq. (6), and is given by Eq. (7).

To complete the specification of the problem, we note that the density associated with each subband and spin orientation is given by

$$n_n^{\sigma}(z)=n_n^{\sigma}|\phi_n^{\sigma}(z)|^2, \tag{35}$$

where n_n^{σ} is the occupancy of each level, which at zero temperature is given by

$$n_n^{\sigma}=N_0(\varepsilon_F-\varepsilon_n^{\sigma})\Theta(\varepsilon_F-\varepsilon_n^{\sigma}). \tag{36}$$

The total electron density may be written

$$n(z)=\sum_{n\sigma} n_n^{\sigma}(z), \tag{37}$$

which implies that the Fermi level E_F is implicitly determined by the condition

$$N_s=\int_{-\infty}^{\infty}dz\,n(z)=\sum_{n\sigma} n_n^{\sigma} \tag{38}$$

[cf. Eqs. (8)–(12)]. The self-consistent solution of these equations proceeds exactly as in the LDA case with the difference that now, in each iteration, one has to solve two Kohn-Sham equations, Eq. (28), for the two spinor components of the wave functions, ϕ_n^{σ}.

B. Self-consistent Hartree-Fock theory

While conventional density-functional theory is a fairly accurate method for determining the properties of semiconductor heterostructures in their paramagnetic and ferromagnetic phases, it is unable to address more complicated magnetic ordering such as antiferromagnetism. To study such phases, it is useful to return to a model Hamiltonian of the electronic system and search for the existence of broken-symmetry states within a mean-field theory. In some cases, such as superconductivity, the mean-field theory gives a quantitative account of these phases.[47] More commonly, however, it sacrifices quantitative accuracy in favor of qualitative insight. This insight manifests itself not only in a physical intuition about the nature of the ground state, but also in the ability to study the distinctive features of the broken-symmetry phase, which may serve as a guide for interpreting experimental data in these systems. We adopt this point of view in what follows.

To that end, consider a three-dimensional electron gas interacting through a potential $V(\mathbf{R}-\mathbf{R}')$ and confined along the z direction by a potential $V_{\rm CONF}(z)$. A confining potential of this type is shown in Fig. 1 for a double quantum well, but the precise shape is unimportant for the development of the formalism. Given a particular $V_{\rm CONF}(z)$, one can construct its eigenfunctions $\xi_n(z)$ and eigenenergies ϵ_n, $n=1,2,3\ldots$, by solving the time-independent Schrödinger equation

$$\left[-\frac{\hbar^2}{2m^*}\frac{d^2}{dz^2}+V_{\rm CONF}(z)\right]\xi_n(z)=\epsilon_n\xi_n(z). \tag{39}$$

In terms of these eigenfunctions, the quasiparticle annihilation operator $\psi_\sigma(\mathbf{R})$ can be written as

$$\psi_\sigma(\mathbf{R})=\frac{1}{\sqrt{A}}\sum_{n\mathbf{k}} e^{i\mathbf{k}\cdot\mathbf{r}}\xi_n(z)c_{n\mathbf{k}\sigma}, \tag{40}$$

where $\mathbf{R}=(\mathbf{r},z)=(x,y,z)$ and $\mathbf{k}=(k_x,k_y)$, A is the transverse area of the sample, and $c_{n\mathbf{k}\sigma}$ annihilates a quasiparticle in subband n, of transverse wave vector $\mathbf{k}$, and with spin projection σ (these conventions will be used throughout this paper). Note that, unlike the density-functional approach, the total confining potential $V_{\rm CONF}(z)$ is specified at the outset and is not determined self-consistently.

Defining a composite subband and spin index $a=(n_a,\sigma_a)$ with summation over repeated indices implied, the Hamiltonian may be written in the basis defined by Eq. (40) as

$$H=H_0+H_{\rm int}=\sum_{\mathbf{k}}\epsilon_{a\mathbf{k}}c^\dagger_{a\mathbf{k}}c_{a\mathbf{k}} + \frac{1}{2A}\sum_{\mathbf{kk'q}}V_{ad,bc}(\mathbf{q})c^\dagger_{a\mathbf{k}+\mathbf{q}}c^\dagger_{b\mathbf{k}'-\mathbf{q}}c_{c\mathbf{k}'}c_{d\mathbf{k}}. \tag{41}$$

In this expression, the quasiparticle energy

$$\epsilon_{a\mathbf{k}}=\epsilon_n+\frac{\hbar^2k^2}{2m^*}-\mu \tag{42}$$

is measured with respect to the chemical potential μ, and the matrix elements of the interaction are

$$V_{ab,cd}(\mathbf{q})=\delta_{\sigma_a\sigma_b}\delta_{\sigma_c\sigma_d}\int\frac{d\mathbf{R}\,d\mathbf{R}'}{A}e^{i\mathbf{q}\cdot(\mathbf{r}-\mathbf{r}')}\xi^*_{n_a}(z)\xi_{n_b}(z) \times V(\mathbf{R}-\mathbf{R}')\xi^*_{n_c}(z')\xi_{n_d}(z'). \tag{43}$$

Our goal is to solve this model within the mean-field theory, allowing for the possibility of broken-symmetry phases. For reasons that will be discussed in Sec. V, we shall restrict attention to those ground states which are translationally invariant transverse to the layering direction, but we shall allow for off-diagonal order in both the subband and spin indices. This assumption excludes from the outset the study of intrawell charge- or spin-density waves and Wigner crystallization, and it is also implicit in the density-functional calculations discussed in Sec. II A. One could modify our treatment to include such phases, but the present model is sufficient for the purposes of exploring the effects of the interwell degrees of freedom. The assumption of translational invariance implies conservation of the transverse wave vector, and so the quasiparticle propagator can be written

$$G_{ab}(k_n)=-\int_0^\beta d\tau e^{i\omega_n\tau}\langle T_\tau[c_{a\mathbf{k}}(\tau)c^\dagger_{b\mathbf{k}}(0)]\rangle, \tag{44}$$

where $k_n=(\mathbf{k},i\omega_n)$, $\beta=1/T$ ($\hbar=k_B=1$ throughout this paper), and the rest of the notation is standard.[48]

The mean-field theory for our model is constructed by using this propagator to compute the electronic self-energy in the self-consistent Hartree-Fock approximation. This approximation corresponds to expanding the self-energy to one-loop order in the interaction and is shown diagrammatically in Fig. 2(a). The resulting self-energy is

$$\Sigma_{ab}(\mathbf{k})=\frac{T}{A}\sum_{k'_m}e^{-i\omega_m0^-} \times[V_{ab,dc}(\mathbf{0})-V_{ac,db}(\mathbf{k}-\mathbf{k}')]G_{cd}(k'_m). \tag{45}$$

The self-consistency of this approximation arises because the propagators used in Eq. (45) are dressed by the same self-energy according to the Dyson equation

$$[(i\omega_n-\epsilon_{a\mathbf{k}})\delta_{ab}-\Sigma_{ab}(\mathbf{k})]G_{bc}(k_n)=\delta_{ac}. \tag{46}$$

To completely specify the system of equations, the chemical potential is determined from the band-filling constraint

$$N_s=\frac{T}{A}\sum_{k_m}e^{-i\omega_m0^-}G_{aa}(k_m). \tag{47}$$

An alternative form of these equations, which will turn out to be convenient for future work, is obtained by inverting the Dyson equation for the interacting propagator $G_{ab}(k_n)$ [Eq. (46)] by making an appropriate choice of the basis. From Eqs. (43) and (45), the matrix $\epsilon_{a\mathbf{k}}\delta_{ab}+\Sigma_{ab}(\mathbf{k})$ is Hermitian, and so possesses a complete and orthonormal set of eigenfunctions $\varphi^c_a(\mathbf{k})$. These eigenfunctions satisfy the eigenvalue equation

$$[\epsilon_{a\mathbf{k}}\delta_{ab}+\Sigma_{ab}(\mathbf{k})]\varphi^c_b(\mathbf{k})=E^c(\mathbf{k})\varphi^c_a(\mathbf{k}) \tag{48}$$

(no sum on c) and the orthonormality relations

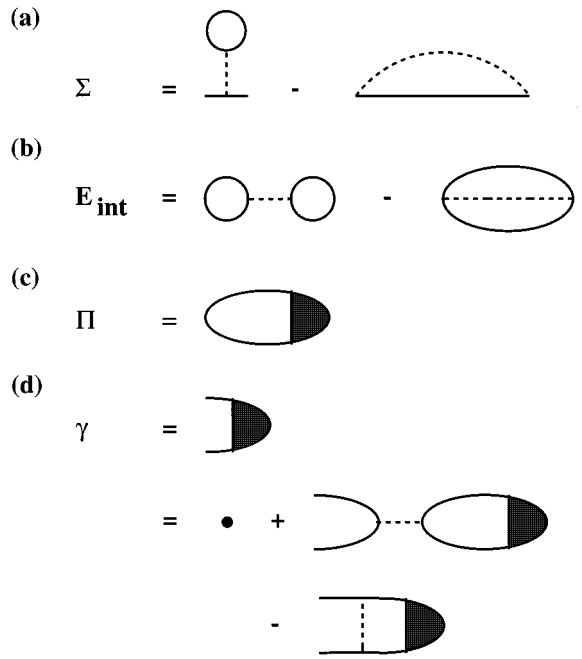

FIG. 2. Many-body diagrams used to compute (a) the self-energy Σ, (b) the contribution of the interactions to the energy $E_{\rm int}=\langle H_{\rm int}\rangle$, (c) the generalized polarizability Π, and (d) the vertex function γ within the self-consistent Hartree-Fock approximation. The solid lines represent dressed electronic propagators [Eq. (44)] and the dashed lines the effective interaction V [Eq. (43)], both of which are matrices in subband and spin space. In order to treat both spin and charge polarizabilities with the same equations, the polarizability is not separated into reducible and irreducible parts.

$$\varphi_a^c(\mathbf{k})\varphi_b^{*c}(\mathbf{k})=\delta_{ab} \tag{49}$$

and

$$\varphi_c^a(\mathbf{k})\varphi_c^{*b}(\mathbf{k})=\delta^{ab}. \tag{50}$$

Equation (46) is diagonal in the basis of these eigenfunctions by construction, so we may invert the equation to obtain

$$G_{ab}(k_n)=\frac{\varphi_a^c(\mathbf{k})\varphi_b^{c*}(\mathbf{k})}{i\omega_n-E^c(\mathbf{k})}. \tag{51}$$

Substituting this relation back into the equation for the self-energy [Eq. (45)], and performing the sum over Matsubara frequencies yields

$$\Sigma_{ab}(\mathbf{k})=\frac{1}{A}\sum_{\mathbf{k}'}\left[V_{ab,dc}(\mathbf{0})-V_{ac,db}(\mathbf{k}-\mathbf{k}')\right]\times\varphi_c^e(\mathbf{k}')\varphi_d^{*e}(\mathbf{k}')f(E^e(\mathbf{k}')), \tag{52}$$

where $f(x)=1/(e^{\beta x}+1)$ is the Fermi function. The band filling constraint Eq. (47) may similarly be written

$$N_s=\frac{1}{A}\sum_{c\mathbf{k}} f(E^c(\mathbf{k}))\equiv\sum_c n^c. \tag{53}$$

Equations (48)–(53) are the equations we will ultimately solve for a simple model interaction in Sec. V A.

The eigenfunctions $\varphi_a^c(\mathbf{k})$ and eigenenergies $E^c(\mathbf{k})$ of the operator $\epsilon_{a\mathbf{k}}\delta_{ab}+\Sigma_{ab}(\mathbf{k})$ are the wave functions and energies of the quasiparticles of the interacting system within self-consistent Hartree-Fock theory. An alternative way of saying the same thing is that we have performed a mean-field decomposition of the Hamiltonian, and diagonalized the result with a Bogoliubov transformation in the particle-particle channel. The annihilation operators for the interacting quasiparticles $\gamma_{\mathbf{k}}^c$ are therefore obtained from the bare operators via $\gamma_{\mathbf{k}}^c=\varphi_a^c(\mathbf{k})c_{a\mathbf{k}}$.

In addition to the physical insight afforded by rewriting the self-energy equations in terms of these functions, the calculation of the energy, entropy, and specific heat of the system becomes straightforward. The energy is the expectation value of the Hamiltonian [Eq. (41)], with the energy shift due to the chemical potential removed:

$$E=\langle H+\mu N\rangle=\langle H_0\rangle+\langle H_{\rm int}\rangle+\mu N_s. \tag{54}$$

Within our self-consistent Hartree-Fock theory, the contribution to the energy from the interaction term in the Hamiltonian is shown graphically by the diagrams in Fig. 2(b). These diagrams lead to the result

$$\langle H_{\rm int}\rangle=\frac{T}{2}\sum_{k_n} e^{-i\omega_n 0^-}G_{ba}(k_n)\Sigma_{ab}(\mathbf{k}), \tag{55}$$

which allows us to write Eq. (54) as

$$E=\frac{T}{2}\sum_{k_n} e^{-i\omega_n 0^-}[2\epsilon_{a\mathbf{k}}\delta_{ab}+\Sigma_{ab}(\mathbf{k})]G_{ba}(k_n)+\mu N_s. \tag{56}$$

Substituting Eq. (51) into this equation, using the eigenequation Eq. (48) and orthonormality relation Eq. (50), and performing the Matsubara sum, the total energy becomes

$$E=\tfrac{1}{2}\sum_{\mathbf{k}}\left[|\phi_a^c(\mathbf{k})|^2\epsilon_{a\mathbf{k}}+E^c(\mathbf{k})\right]f(E^c(\mathbf{k}))+\mu N_s. \tag{57}$$

The entropy in the interacting basis is simply the standard free-fermion result

$$S=-\sum_{\mathbf{k}}\{f(E^c(\mathbf{k}))\ln f(E^c(\mathbf{k}))+[1-f(E^c(\mathbf{k}))]\times\ln[1-f(E^c(\mathbf{k}))]\}, \tag{58}$$

and the specific heat is obtained directly from this equation:

$$C_V=T\frac{\partial S}{\partial T}=\sum_{\mathbf{k}}\left(-\frac{\partial f(E^c(\mathbf{k}))}{\partial E^c(\mathbf{k})}\right)\beta E^c(\mathbf{k})\frac{d(\beta E^c(\mathbf{k}))}{d\beta}. \tag{59}$$

In order to get a full picture of the interacting system, one must go beyond the single-particle properties and thermodynamic functions, and examine the response of the system to external perturbation. As discussed in Sec. II A 1, resonant inelastic light scattering has proven to be a powerful tool for studying the charge- and spin-density excitations in semiconductor heterostructures. Consequently, we will focus on the generalized density response function and the resulting collective excitations which can be observed in these experiments. As in Sec. II A 1, we will not compute the form factors necessary to connect the polarizability to the inelastic light-scattering cross section; we merely note that the collective modes we will discuss are detectable in these experi-

ments with a particular (and structure-dependent) arrangement of scattering angles, polarizations, etc.

We begin by defining a generalized density operator

$$\rho^{\mu}(\mathbf{R}) = \psi^{\dagger}_{\sigma_1}(\mathbf{R})\sigma^{\mu}_{\sigma_1\sigma_2}\psi_{\sigma_2}(\mathbf{R}), \tag{60}$$

where $\sigma^{\mu} = \{\sigma^0,\sigma^1,\sigma^2,\sigma^3\} = \{1,\sigma^x,\sigma^y,\sigma^z\}$. Note that the number density $n(\mathbf{R}) = \rho^0(\mathbf{R})$ and the spin density $s^i(\mathbf{R}) = (\hbar/2)\rho^i(\mathbf{R})$, $i = 1$, 2, or 3. Suppose we can couple to this density through an external force $F^{\mu}_{\rm ext}(\mathbf{R},t)$ which adds a term

$$H_{\rm ext}(t) = -\int d\mathbf{R}\ \rho^{\mu}(\mathbf{R},t)F^{\mu}_{\rm ext}(\mathbf{R},t) \tag{61}$$

to the Hamiltonian (a sum on μ is implied). The linear response of the generalized density to this perturbation is then given by[49]

$$\langle \delta\rho^{\mu}(\mathbf{R},t)\rangle = i\int d\mathbf{R}'dt'\,\theta(t') \times\langle[\rho^{\mu}(\mathbf{R},t),\rho^{\nu}(\mathbf{R}',t')]\rangle F^{\nu}_{\rm ext}(\mathbf{R}',t'), \tag{62}$$

where the angle brackets denote the thermodynamic average in the absence of $H_{\rm ext}(t)$.

As mentioned above, we assume that the interacting system is translationally invariant in the transverse direction, and it is also time-translation invariant. Thus we may introduce partial Fourier transforms

$$\rho^{\mu}(\mathbf{R},t) = \frac{1}{A}\sum_{\mathbf{q}}\int\frac{d\omega}{2\pi}e^{i(\mathbf{q}\cdot\mathbf{r}-\omega t)}\rho^{\mu}(\mathbf{r},z,t), \tag{63}$$

and write Eq. (62) as

$$\langle \delta\rho^{\mu}(\mathbf{q},z,\omega)\rangle = i\int dz'dt'e^{i\omega t'}\theta(t') \times\langle[\rho^{\mu}(\mathbf{q},z,t),\rho^{\nu}(-\mathbf{q},z',t')]\rangle \times F^{\nu}_{\rm ext}(\mathbf{q},z',\omega). \tag{64}$$

From Eqs. (40) and (60), we can rewrite the Fourier components of the density operator as

$$\rho^{\mu}(\mathbf{q},z) = \xi^{*}_{n_a}\xi_{n_b}\sigma^{\mu}_{\sigma_a\sigma_b}\mu\rho_{ab}(\mathbf{q}), \tag{65}$$

with

$$\rho_{ab}(\mathbf{q}) = \sum_{\mathbf{k}} c^{\dagger}_{a\mathbf{k}}c_{b\mathbf{k}+\mathbf{q}}. \tag{66}$$

Using this relation, we obtain the final form for the generalized density response,

$$\langle \delta\rho^{\mu}_{ab}(\mathbf{q},\omega)\rangle = -\Pi_{ab,cd}(\mathbf{q},\omega)F^{\rm ext}_{cd}(\mathbf{q},\omega), \tag{67}$$

where

$$\Pi_{ab,cd}(\mathbf{q},\omega) = -i\int dt e^{i\omega t}\langle[\rho_{ab}(\mathbf{q},t),\rho^{\dagger}_{cd}(\mathbf{q},0)]\rangle, \tag{68}$$

$$\langle \delta\rho^{\mu}(\mathbf{q},z,\omega)\rangle = \xi^{*}_{n_a}(z)\xi_{n_b}(z)\sigma_{\sigma_a,\sigma_b}\mu\langle\delta\rho_{ab}(\mathbf{q},\omega)\rangle, \tag{69}$$

and

$$F^{\rm ext}_{cd}(\mathbf{q},\omega) = \int dz'\,\xi_{n_c}(z')\xi^{*}_{n_d}(z')\sigma^{\nu}_{\sigma_c\sigma_d}F^{\nu}_{\rm ext}(\mathbf{q},z',\omega). \tag{70}$$

In order to obtain the subband- and spin-resolved polarizability [Eq. (68)], we compute the polarizability in Matsubara frequencies $i\nu_n = 2\pi nT$,

$$\Pi_{ab,cd}(q_n) = -\int_0^{\beta} d\tau e^{i\omega_n\tau}\langle T_{\tau}[\rho_{ab}(\mathbf{q},\tau)\rho^{\dagger}_{cd}(\mathbf{q},0)]\rangle \tag{71}$$

($q_n = (\mathbf{q}, i\nu_n)$), and analytically continue to real frequencies by the conventional substitution $i\nu_n \rightarrow \Omega + i\delta$ (cf. Ref. 48). This polarizability is calculated within a conserving approximation[50] using the diagrams shown in Figs. 2(c) and 2(d). These diagrams yield the expressions

$$\Pi_{ab,cd}(q_n) = \frac{T}{A}\sum_{k_m} G_{ea}(k_m)G_{bf}(k_m+q_n)\gamma_{ef,cd}(k_m,k_m+q_n) \tag{72}$$

for the polarizability, and

$$\gamma_{ab,cd}(k_m,k_m+q_n) = \delta_{ac}\delta_{bd} - \frac{T}{A}\sum_{k'_l}[V_{bf,ea}(\mathbf{k}-\mathbf{k}') - V_{ba,ef}(\mathbf{q})] \times G_{ge}(k'_l)G_{fh}(k'_l+q_n)\gamma_{gh,cd}(k'_l,k'_l+q_n) \tag{73}$$

for the vertex function. Contrary to the usual convention, we include the RPA screening diagrams in the vertex function, and thus do not distinguish between reducible and irreducible polarizabilities. The reason is that, in the broken-symmetry phases we will examine, the propagators are no longer diagonal in spin, so these screening terms enter into both the spin- and charge-density response functions, reducing the usefulness of the division between reducible and irreducible polarizabilities. Note that even these approximate equations for the polarizability must be solved numerically for a general interaction. If the interaction is wave vector independent, on the other hand, the vertex equation can be solved simply (cf. Sec. V).

The interpretation of the polarizability as a response function can be used to visualize the real-space density fluctuations it describes. If one perturbs the system with the external force $F^{\mu}_{\rm ext}(\mathbf{R},t) \propto e^{i(\mathbf{q}\cdot\mathbf{r}-\omega t)}$, Eqs. (62)–(70) imply that the response in real space will be

$$\langle \delta\rho^{\mu}(\mathbf{R},t)\rangle \propto e^{i(\mathbf{q}\cdot\mathbf{r}-\omega t)}\xi^{*}_{n_a}(z)\xi_{n_b}(z)\sigma^{\mu}_{\sigma_a}\sigma_b\Pi_{ab,cd}(\mathbf{q},\omega)f^{\rm ext}_{cd}, \tag{74}$$

where $f^{\rm ext}_{cd}$ is related to how this force perturbs the subband and spin indices. For example, to examine the spin-density response between the lowest two subbands,

$$f^{\rm ext}_{cd} = [\delta_{n_c1}\delta_{n_d2} + \delta_{n_c2}\delta_{n_d1}]\delta_{\sigma_c\uparrow}\delta_{\sigma_d\downarrow}. \tag{75}$$

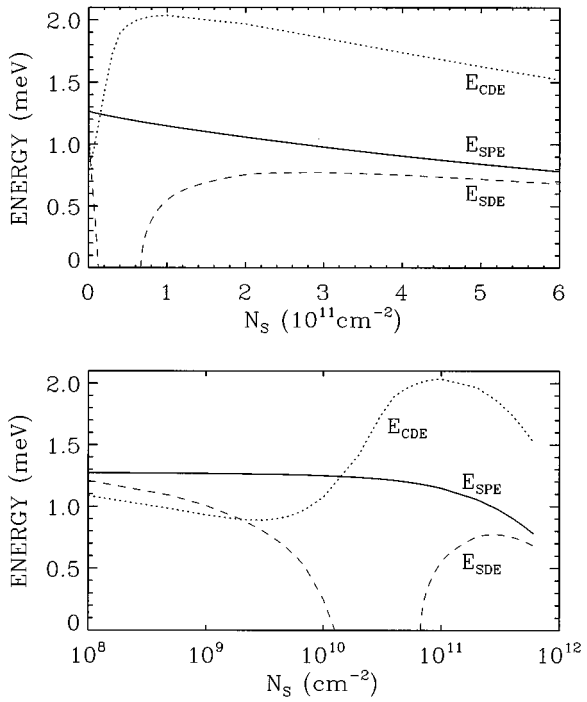

FIG. 3. Calculated intersubband charge-density excitation E_{CDE}, spin-density excitation E_{SDE}, and single-particle excitation $E_{\mathrm{SPE}} \equiv \triangle_{\mathrm{SAS}}$ energies as functions of the 2D electron density N_{S} for a DQW structure with barrier width $d_B = 40$ Å and well width $d_W = 139$ Å. The critical density for the instability $N_{\mathrm{C}} \approx 0.69 \times 10^{11}$ cm^{-2}. The bottom figure shows an expanded density range, making obvious the reentrance of the normal phase at very low electron density.

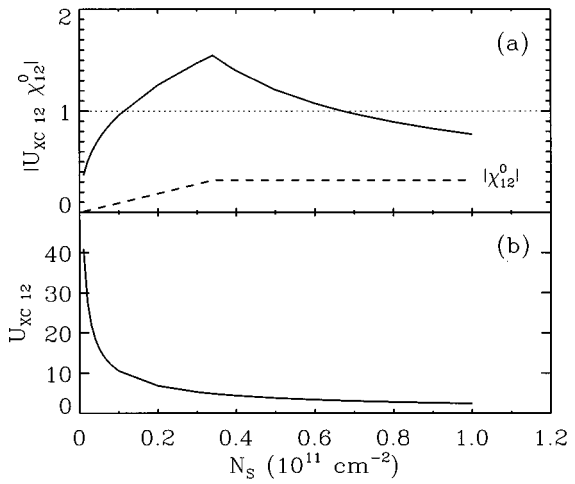

FIG. 4. Dependence on the sheet density N_S of (a) the mean-field vertex correction $|U_{\mathrm{XC}\,12}\chi^0_{12}|$ (solid line) and the absolute value of the lowest-order polarizability $|\chi^0_{12}|$ (dashed line), and (b) the spin-polarized exchange-correlation-induced vertex correction $U_{\mathrm{XC}\,12}$ for the double-quantum-well structure in Fig. 1. Note that the electron gas is unstable in the range of densities where $|U_{\mathrm{XC}}\chi^0_{12}| \geqslant 1$ (see text).

This procedure works for general wave vector and frequency, but has special significance when these quantities correspond to a collective-mode of the system, in which case the response gives the polarization of the collective mode. Note that, since the response function diverges at a collective excitation, in practice one applies this formula by adding a small imaginary part to the frequency to control this divergence. As with the equations for the polarizability, this numerically intensive approach for obtaining the collective-mode polarization is required for the broken-symmetry phases where the off-diagonal terms make an analytic calculation difficult.

III. INTERSUBBAND INSTABILITIES

In this section, we shall study the instabilities of an electron gas confined to coupled double-quantum-well (DQW) and wide single-quantum-well structures by examining their intersubband collective excitations. We begin by applying the formalism described in Sec. II A to the typical GaAs/$Al_xGa_{1-x}As$ DQW structure shown in Fig. 1; similar samples were used in the experimental study of Ref. 21. Although our TDLDA calculation includes all the subband energies shown in the figure, we are only concerned with intersubband transitions between the lowest two subbands (subbands 1 and 2), whose typical separation $\Delta_{\mathrm{SAS}} \equiv \varepsilon_2 - \varepsilon_1 \approx 1$ meV (SAS is symmetric-antisymmetric). The exact values of Δ_{SAS} are plotted in Fig. 3, along with the calculated long-wavelength energies of the intersubband collective modes as a function of the sheet density.

Two distinctive features of these collective modes are seen in Fig. 3. The first feature is that the CDE energy becomes less than Δ_{SAS} around $N_s \approx 0.2 \times 10^{11}$ cm^{-2}. This behavior, originally predicted in Ref. 19 for single quantum wells, has recently been verified experimentally,[23] and will not be discussed further. The second—and for our purposes more important—feature is that the intersubband SDE energy goes to zero below a critical density $N_C \approx 0.7 \times 10^{11}$ cm^{-2} and becomes finite again below 0.1×10^{11} cm^{-2}. This softening of the intersubband SDE mode indicates that the normal system with a ''metallic'' Fermi surface is unstable at or below N_C, since it can spontaneously create spin-reversed intersubband electron-hole pairs (''triplet excitons'') at no cost in energy. We conclude that there is a phase transition in this DQW at the critical sheet density N_C from the normal 2D electron liquid to a triplet intersubband exciton liquid, and that the system reenters the normal phase at a lower density. This electronic phase transition is due exclusively to exchange-correlation effects which make the vertex correction or excitonic shift larger than Δ_{SAS} [Eq. (25)] and thus cause the SDE to collapse. The reentrance of the normal phase at lower density is simply explained by the fact that the vertex correction vanishes as $N_s \to 0$ according to Eq. (25). We note that the transition to a Wigner crystal occurs at much lower N_s values than those considered in this paper and so does not account for the SDE collapse.[18,44]

Additional evidence in support of the excitonic transition comes from the density dependence of the mean-field vertex correction $|U_{\mathrm{XC}}\chi^0_{12}|$, which is plotted in Fig. 4(a). This vertex correction consists of the spin-polarized, exchange-correlation-induced vertex function U_{XC} [Fig. 4(b)] and the uncorrected intersubband polarizability $\chi^0_{12} \equiv \Pi^0_{12} + \Pi^0_{21}$ [Fig. 4(a)]. In the two-subband limit, the vertex-corrected irreducible response function is given by $\chi^0_{12}[1 - U_{\mathrm{XC}}\chi^0_{12}]^{-1}$, which

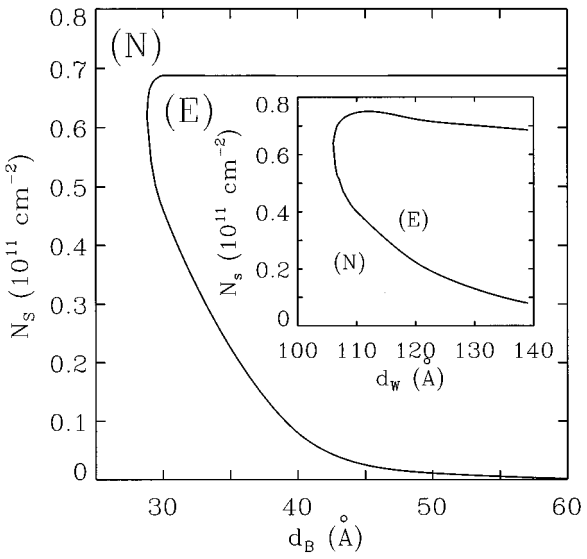

FIG. 5. Calculated zero-temperature phase diagram for double quantum wells in terms of the sheet density N_S and the barrier width d_B for fixed well widths $d_W = 139$ Å. Inset: phase diagram for fixed $d_B = 40$ Å in terms of the sheet density and well widths. The normal (N) and the triplet excitonic (E) phases are shown.

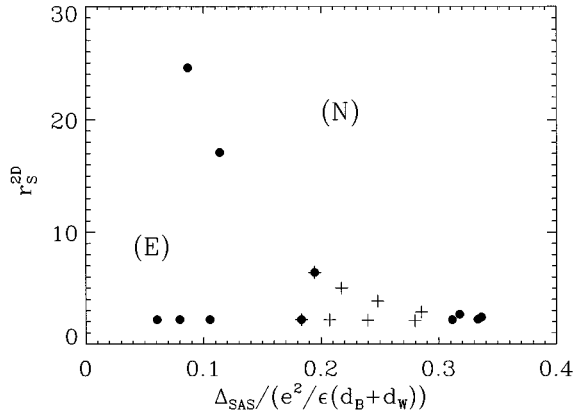

FIG. 6. Calculated zero-temperature phase diagram for coupled double quantum wells in terms of $r_s^{2D} \equiv (\pi N_S)^{-1/2}/a_0$ and the dimensionless symmetric-antisymmetric subband splitting $\Delta_{SAS}/(e^2/\epsilon(d_W+d_B))$, where a_0 and ϵ are the Bohr radius and dielectric constant for GaAs and d_B (d_W) is the barrier (well) width. Solid circles correspond to $d_W = 139$ Å and various d_B, and are taken from the main part of Fig. 5, while the crosses correspond to $d_B = 40$ Å and various d_W and are obtained from the inset to Fig. 5. The normal (N) and the triplet excitonic (E) phases are shown.

clearly has an instability when $|U_{XC}\chi^0_{12}| \geq 1$ [cf. Eq. (24)]. As shown in Fig. 4(a), this ''Stoner criterion'' is satisfied in the range of sheet densities in which the SDE has collapsed.

Having established the existence of the SDE-collapsed phase for a particular DQW structure, we can vary the geometry of the structure to study the persistence of this phase. For well widths fixed at 139 Å, the calculated zero-temperature phase diagram in terms of the sheet density and barrier width d_B is shown in Fig. 5. For very small barrier widths, Δ_{SAS} is too large for the vertex correction to overcome it, even at low densities, making the normal phase the only stable phase. For very large barrier widths, on the other hand, Δ_{SAS} is exponentially small, and the normal phase gives way to the excitonic one at extremely low densities. Of course, for such exponentially small Δ_{SAS}, the critical temperature for our predicted instability is also exponentially low, implying that the phase transition in large-d_B, low-density DQW structures would be unobservable in practice.[51] At higher densities in the large-d_B structures, the normal phase reasserts itself due to the diminishing influence of the vertex correction. For intermediate values of the barrier width, we see the reentrant behavior described above with an upper critical density that is nearly independent of the barrier width. A similar phase diagram is obtained when the barrier width is fixed at 40 Å and the well widths are varied, as demonstrated by the inset to Fig. 5. By expressing the sheet density and Δ_{SAS} in dimensionless form, the data from Fig. 5 can be reduced to the universal zero-temperature phase diagram shown in Fig. 6. From this figure, we see quite clearly that the excitonic phase appears in a range of densities below a critical symmetric-antisymmetric splitting Δ_{SAS}, and that this density range increases as Δ_{SAS} decreases.

The results discussed so far for the intersubband SDE energy are for zero in-plane momentum transfer. Figure 7 shows the dispersion relation of the lowest intersubband spin-density mode for several sheet densities N_s above N_C. The most important feature shown is that the SDE mode becomes soft at a finite value of the in-plane momentum transfer, q_c, at a critical density somewhat higher than the critical density found at zero in-plane momentum transfer. The critical momentum is given by $q_c = k_{F1} - k_{F2}$, where k_{Fi} is the in-plane Fermi wave vector of the ith subband in the normal state. This indicates that the excitonic instability,

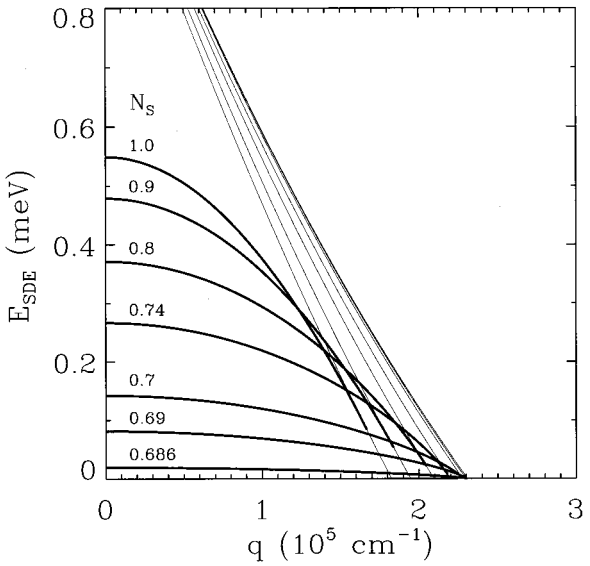

FIG. 7. Energy of the intersubband spin-density excitations E_{SDE} as a function of wave vector q in a coupled double-quantum-well system with a barrier width of 40 Å and well widths of 139 Å for sheet densities N_S in units of 10^{11} cm^{-2} approaching the critical density $N_C \simeq 0.686 \times 10^{11}$ cm^{-2} from above (thick lines). The thin lines show the lower boundary of the particle-hole continuum, above which the collective excitations are Landau damped.

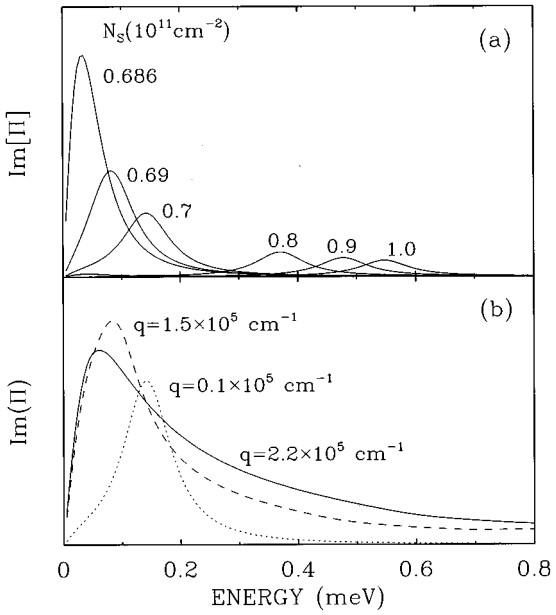

FIG. 8. Calculated Raman-scattering spectra in the cross-polarization geometry for a double-quantum-well structure with a 40-Å barrier width and 139-Å well widths. The curves illustrate the signatures of the excitonic instability (a) as the sheet density N_S is lowered to the critical density, and (b) as the wave-vector transfer q is increased at constant sheet density $N_S=0.7\times10^{11}$ cm^{-2}.

for densities slightly above N_C, may occur at a finite value of in-plane q, a point to which we shall return in Secs. V B and VI.

Thus, we expect that a softening of the intersubband SDE may be observed either at fixed q and varying N_s [cf. Fig. 8(a)] or for $q\rightarrow q_c$ at certain fixed values of N_s [cf. Fig. 8(b)]. In Fig. 8(a), we show the spectral function of the intersubband spin-density excitations as the instability is approached from the high-density side at very small q. As N_s approaches N_C, the spectral peak shifts toward zero energy, and the line narrows. On the other hand, the approach to the critical momentum transfer q_c at densities just above N_C, presented in Fig. 8(b) for $N_s=N_C=0.7\times10^{11}$ cm^{-2} at various values of q approaching q_c, the line broadens as it softens. These spectra are similar to what would be observed in Raman-scattering experiments in the cross-polarization geometry.[29,15,16,21] For sheet densities within the SDE-collapsed phase, the TDLDA treatment employed in the section breaks down, and we must employ the techniques of Sec. II B to determine the collective modes, which we shall do in Sec. V.

Finally, we mention that the instability discussed here for DQW's can also happen in wide *single* quantum wells, in which the effective potential develops a barrier in the center at moderate densities, becoming similar to a DQW.[7] An example of this phenomenon is illustrated in Fig. 9; notice that the electron density profile is similar to that for the DQW system shown in Fig. 1. In this *effective* double-well system, the separation between the two lowest-lying subbands is small, about 0.2 meV, as in the coupled DQW's, and the possibility of a suppression of the intersubband SDE's by the vertex correction arises. A calculation of the SDE energies shows that this is indeed the case, as can be seen in Fig. 10.

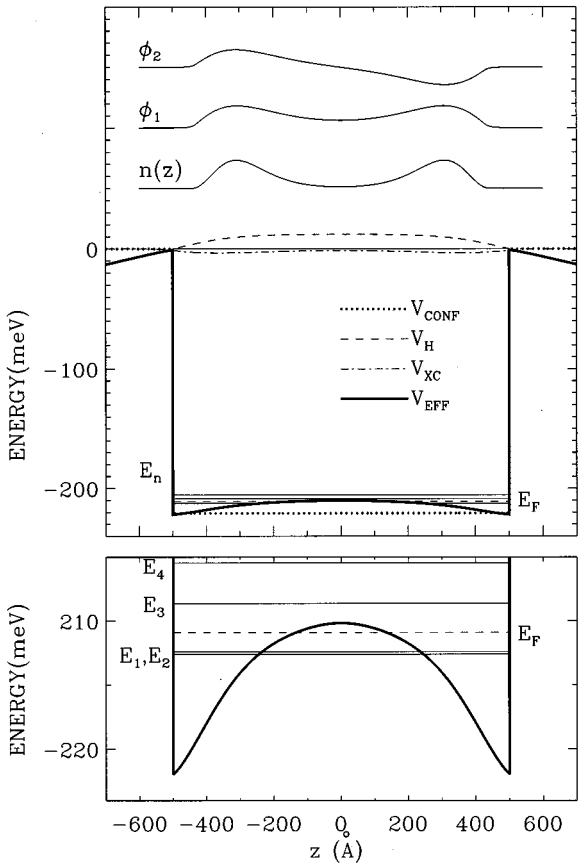

FIG. 9. Typical wide square quantum well given by the bare confining potential $V_{\rm CONF}$, and its self-consistent LDA subband energy levels E_n, eigenfunctions ϕ_n, electron density $n(z)$, Fermi energy E_F, and effective, Hartree, and exchange-correlation potentials $V_{\rm EFF}$, V_H, and $V_{\rm XC}$. The sheet density is $N_s=0.9\times10^{11}$ cm^{-2}. The figure shows how the electronic density profile becomes localized on the sides of the well, similar to the profile in a double quantum-well system. Bottom: lowest energies in expanded scale.

For the square well considered, whose width is 1000 Å, the region in which the SDE has collapsed is somewhat smaller than that for the DQW of Fig. 1 with a 40-Å barrier width, but it occurs around the same $N_s\sim0.4\times10^{11}$ cm^{-2}. Hence inelastic light-scattering experiments should be able to detect the SDE instability in wide square wells also.

IV. FERROMAGNETIC PHASE

In Sec. III, we showed that an electron gas confined in a coupled double-quantum-well structure has an instability which is indicated by the vanishing of the energy of the intersubband spin-density excitations. One of the goals of this section is to establish whether this instability corresponds to a phase transition from the normal spin-unpolarized (paramagnetic) ground state to a spin-polarized (ferromagnetic) one. A second goal is to employ the LSDA formalism of Sec. II A 2 to the ferromagnetic phase transition in single square quantum wells. In particular, we are interested in the dependence of the critical density on the well width, as it would reveal an aspect of the crossover from two- to three-dimensional behavior of the electron gas

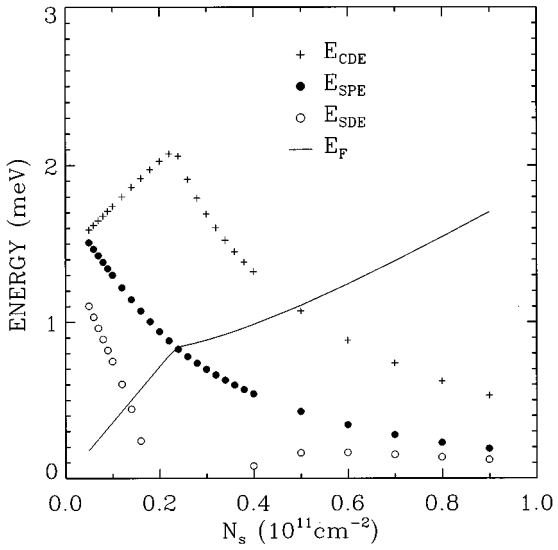

FIG. 10. Calculated intersubband charge-density excitation energy E_{CDE}, spin-density excitation energy E_{SDE}, and single-particle excitation energy $E_{\mathrm{SPE}} \equiv \Delta_{\mathrm{SAS}}$ as functions of the 2D electron density N_S for the wide square-well structure shown in Fig. 9. Note the collapse of E_{SDE} for $N_S \simeq 0.2-0.4\times 10^{11}$ cm^{-2}.

which, to our knowledge, has not been explored in the past. Our main finding is that the LSDA does predict a ferromagnetic transition in single quantum wells and, moreover, that as the electron gas is widened the transition density decreases (the ferromagnetic phase becomes less favorable). This dependence of the critical density on the electron-layer width agrees with the well-known fact that the influence of the Coulomb interaction is stronger for lower dimensionality.

We first determine whether the excitonic instability studied in Sec. III can be explained in terms of a ferromagnetic transition, that is, a transition from the usual spin-unpolarized ground state to a partially or fully polarized one. We concentrate on a coupled double-quantum-well system in which each individual square well is 139 Å wide and the well separation is 40 Å—the main structure studied in Sec. III. As in the better-known 3D case, a fully polarized phase is expected at low density, and a normal, unpolarized phase at high density. To compute the spin polarization of the system at a given sheet density N_s within the iterative, self-consistent LSDA method, it should be enough, in principle, to introduce a slight asymmetry in the initial choice of spin densities. If the correct ground state were unpolarized, the initial asymmetry would rapidly disappear in the iteration process. On the other hand, if a polarized state were expected, the initial small polarization would increase until convergence to the fully polarized is achieved. However, since the solution of the self-consistent set of equations of the LSDA method is affected by numerical inaccuracies, in practice our algorithm is sensitive to the initial guess for the spin-density profiles. Therefore, we employ the following method to determine the ground-state polarization of the system. For a given density N_s, we solve the self-consistent algorithm starting with the spin densities $n_1^+(z)=\eta n_u(z)$, $n_1^-(z)=(1-\eta)n_u(z)$, $n_2^+(z)=0$, and $n_2^-(z)=0$ for $\eta=0.55$ and 0.95 and $n_u(z)$ the density from the unpolarized LDA calculation (only one subband is occupied at the low N_s studied). If the calculation converges to a polarized or an unpolarized state for both values of η, we take the result as the true polarization at that given N_s. Otherwise, we assume that the result is affected by the insufficient numerical precision.

With this method, we obtain the phase diagram of spin polarization as a function of N_s for the coupled DQW defined above. The calculation converges to a fully polarized state, regardless of the initial choice of spin densities, for $N_s < 4\times 10^8$ cm^{-2}, and to an unpolarized state for $N_s > 1.7\times 10^9$ cm^{-2}. In the range $N_s = 0.4$–1.7×10^9 cm^{-2}, the solution is polarized for the choice $\eta=0.95$, and unpolarized for $\eta=0.55$.

Therefore, our first conclusion is that, within the LSDA, *there is a ferromagnetic transition* as a function of the electron density N_s in a coupled DQW system; for our particular choice of parameters, the transition occurs around $N_s \approx 1\times 10^9$ cm^{-2} at zero temperature. On the other hand, the ferromagnetic transition occurs at a density which is almost two orders of magnitude smaller than the critical density N_C of the excitonic transition of Sec. III. Moreover, it does not seem to show reentrant behavior at lower density as the excitonic transition does. Based on these differences, we conclude that *the ferromagnetic transition cannot be identified as the excitonic phase transition* of Sec. III.

Having achieved the first aim of this section, we now turn to the second, namely, the possibility of ferromagnetism in single square wells. We wish to determine the critical density of the ferromagnetic transition as a function of the well width in order to take the first step in studying the evolution of this transition as a function of the dimensionality of the electron gas. The analytical results for two and three dimensions summarized in Sec. II A 2 indicate that, in 2D, the exchange energy is more important than in 3D, indicating a higher 2D critical density. In quasi-2D systems, we therefore expect that the ferromagnetic critical density should decrease as the well width is increased.

Employing the method described above, we study the ferromagnetic transition in five single square wells of widths $d_W = a_0$, $2a_0$, $4a_0$, $6a_0$, and $8a_0$, where $a_0 = 98.7$ Å is the effective Bohr radius in GaAs. The resulting phase diagram is presented in Fig. 11 in terms of N_s versus well width, and also in terms of the 2D and 3D r_s and well width; the vertical bars give the density range where the polarization of our solution depends on the initial choice of spin densities. As expected, we see that the critical density decreases with increasing well width. However, the limiting values of r_s for narrow, and wide wells cannot be directly compared with the pure two- and three-dimensional Hartree-Fock values for three reasons. First, the analytical results are obtained in the jellium model, whereas in our quantum-well calculations the positive charges of the ionized donors are located far away from the electron gas, which should produce an important change in the direct Coulomb energy and hence affect the ferromagnetic critical density. Second, our calculation includes correlation effects which go beyond the exchange interaction. Third reason to expect differences is that, in the LSDA, exchange is treated in a local and static approximation.

This exchange-correlation potential is obtained from the ground-state energy of a uniform electron gas, which is not

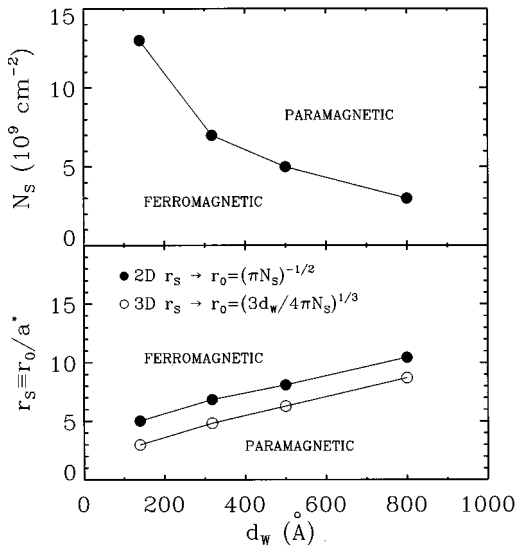

FIG. 11. Approximate zero-temperature, spin-polarization phase diagram of single square wells calculated in the local-spin-density approximation in terms of the sheet density N_S and well width d_B (top) and the r_s parameter and well width (bottom).

known exactly and must be calculated within some approximation scheme. Several authors have proposed different parametrizations of the exchange-correlation potential, which are based on different calculations of the 3DEG ground-state energy and which therefore differ somewhat from each other. We have checked some of our results using the parametrization of Gunnarsson and Lundqvist,[52] which gives a larger difference between the potentials for different spin polarizations than the Ceperley-Alder one, making the ferromagnetic phase more favorable. For example, for the square well of width $d_W=4a_0$, the critical density is 1.3×10^{10} cm^{-2}, ten times higher than with Ceperley Alder. Thus our calculations indicate that within the LSDA a ferromagnetic transition is indeed present in the quasi-two-dimensional electron gas, but the value of the critical density for the transition cannot be accurately determined with this method.

V. ANTIFERROMAGNETIC PHASE

Based on the results of the preceding two subsections, we can draw the following conclusions: (1) double or wide single quantum-well structures can undergo an excitonic instability in a range of densities, and (2) this instability cannot be associated with a ferromagnetic transition. We would like to understand the nature of the ground state of the excitonic phase and determine its excitations, but we see that the density-functional approach cannot assist us further. In order to make progress, we employ the self-consistent Hartree-Fock formalism developed in Sec. II B, which allows us to study ground states with broken symmetries which are not accessible through ordinary density functional theory.

As pointed out in Sec. II B, the self-consistent Hartree-Fock model for systems with a Coulomb interaction is not quantitatively accurate, but should reproduce the qualitative features of the later phase. Our goal is therefore to construct a minimal model of the systems which exhibit the excitonic instability which is still tractable. We can make several observations about the excitonic instability which will guide us in developing this model. First, the instability in the LDA calculations occurs with a *wave-vector-independent* interaction, as seen from the LDA expressions for the irreducible polarizability, Eqs. (13) and (16). Second, the instability is signaled by a soft mode which is an excitation between the lowest two subbands and is accompanied by a spin flip. Thus our minimal model will focus only on the lowest two subbands, allow for off-diagonal terms in the subband and spin indices, and use an interaction which in constant in wave-vector space. In the rest of this section, we discuss the results which follow from this minimal model; a preliminary report of this work has already appeared in the literature.[25]

A. Point-contact model

A **q**-independent interaction has several simplifying consequences. First, as seen from Eq. (45), the self-energy will also be wave-vector independent. From Eq. (48), this result implies that the eigenfunctions $\varphi_a^c(\mathbf{k})$ are also wave vector independent and that the interacting eigenenergies may be written

$$E^c(\mathbf{k})=e^c+\frac{\hbar^2k^2}{2m^*}-\mu. \tag{76}$$

Because these eigenenergies are the energies of the interacting quasiparticles, the effect of the interaction is to shift and/or rearrange the noninteracting bands without destroying their parabolic dispersion. Consequently, the broken-symmetry phases available within this model will not exhibit any energy gap, in contrast to what occurs in superconductivity[47] and in other excitonic transitions which have been studied.[53] The reason for this difference is that the interacting quasiparticles are linear combinations of electrons and holes in the latter cases, whereas in this case they are linear combinations of electrons from different subbands in the former.

Second, the simplest interaction which is **q** independent is a δ function in real space: $V(\mathbf{R})=V\delta(\mathbf{R})$. Inserting this form into Eq. (43) yields

$$V_{ab,cd}(\mathbf{q})=\delta_{\sigma_a\sigma_b}\delta_{\sigma_c\sigma_d}V_{n_an_b,n_cn_d}, \tag{77}$$

with

$$V_{n_an_b,n_cn_d}=V\int dz\,\xi^*_{n_a}(z)\xi_{n_b}(z)\xi^*_{n_c}(z)\xi_{n_d}(z). \tag{78}$$

Making the standard assumption that the quantum-well structure is symmetric, the wave functions $\xi_n(z)$ may be chosen to be real and parity eigenstates. From Eq. (78), these symmetries imply that the order of the subband indices in the matrix elements is irrelevant, and that matrix elements of the form $V_{11,12}$, $V_{12,22}$, and cyclic permutations vanish. Thus there are only three independent matrix elements: $V_{11}=V_{11,11}$, $V_{22}=V_{22,22}$, and $V_{12}=V_{11,22}$ plus permutations. Since we are interested in the minimal model exhibiting the excitonic instability, we will neglect V_{11} and V_{22} in order to focus on the intersubband effects, leaving a model with two free parameters: the sheet density N_s and the intersubband interaction V_{12}.

Applying these approximations to Eq. (52), we find that the self-energy reduces to

$$\Sigma_{n_1\sigma_1,n_2\sigma_2}=V_{n_1n_2,n_3n_4}n^c\begin{cases}\varphi^c_{n_3-\sigma_1}\varphi^{*c}_{n_4-\sigma_1}, & \sigma_1=\sigma_2\\ -\varphi^c_{n_3\sigma_1}\varphi^{*c}_{n_4\sigma_2}, & \sigma_1\neq\sigma_2.\end{cases} \tag{79}$$

This equation is supplemented by the band-filling constraint Eq. (53), with the electron density in each interacting subband given by

$$n^c=\frac{1}{A}\sum_{\mathbf{k}} f(E^c(\mathbf{k})). \tag{80}$$

In addition, the integral equations determining the polarizability [Eqs. (72)–(73)] can be reduced to a matrix equation. The first step in this reduction is to observe that the vertex function γ in Eq. (73) is a function only of q_n when the the interaction has no $\mathbf{q}$ dependence, and satisfies the equation

$$\gamma_{ab,cd}(q_n)=\delta_{ac}\delta_{bd}+[V_{ba,ef}-V_{bf,ea}]\Pi^{(0)}_{ef,gh}(q_n)\gamma_{gh,cd}(q_n), \tag{81}$$

where

$$\Pi^{(0)}_{ab,cd}(q_n)=\frac{T}{A}\sum_{k_m} G_{ca}(k_m)G_{bd}(k_m+q_n) \tag{82}$$

is the polarizability without vertex corrections. In the interacting system, $\Pi^{(0)}_{ab,cd}$ may be written through the use of Eq. (51) as

$$\Pi^{(0)}_{ab,cd}(q_n)=\varphi^{*e}_a\varphi^f_b\varphi^e_c\varphi^{*f}_d\Pi^{ef}(q_n). \tag{83}$$

After analytically continuing to real frequencies, the function $\Pi^{ef}(q)$ is just Eq. (22) with $g_s=1$ and using the interacting energies [Eq. (76)]. Inserting this result into Eq. (72) and rearranging yields

$$[\delta_{ag}\delta_{bh}-\Pi^{(0)}_{ab,ef}(q)(V_{fe,gh}-V_{fh,ge})]\Pi_{gh,cd}(q)=\Pi^{(0)}_{ab,cd}(q). \tag{84}$$

Inverting this matrix equation gives the polarizability. When this equation cannot be inverted for a particular $(\mathbf{q},\omega)$, i.e., when the determinant of the matrix in brackets vanishes, the system exhibits a collective mode. The polarization of these collective modes can be determined by, for example, the method discussed in Sec. II B.

Before proceeding to a discussion of the normal-state properties of our point-contact model, it is appropriate to discuss briefly the question of how well this model approximates reality. The Hartree-Fock approximation is known to be a poor one in the interacting electron gas because it neglects screening effects, but including these effects realistically is a difficult problem which has not yet been resolved. In computing the collective modes, this problem is amplified by the distinction one should draw between the interaction between the bubbles, which is unscreened, and the interaction within the bubbles that gives the nontrivial part of the vertex equation, which should be screened. Summing a particular set of screening diagrams may reduce the error introduced into the self-energy, but would render the collective-mode calculation completely intractable. Thus we adopt a strong approximation to the actual Coulomb interaction, a point-contact interaction, which should reproduce the qualitative features of the screening effects while leaving a solvable set of equations.

B. Normal-state instability

Our goal is to use the point-contact interaction model we have just described as the minimal model for the excitonic instability. It is therefore critical to verify that this model exhibits the instability in its normal state, an exercise which will also provide guidance as to the nature of the broken-symmetry state. The first step in this process is to compute the self-energy and chemical potential in the interacting system. In the normal paramagnetic phase of this model, we know that the wave functions of the subbands are not mixed, and that the band structure consists of two parabolic subbands, each with degenerate spin-up and spin-down components. Consequently, the self-energy is diagonal in subband and spin indices, and the eigenvectors of Eq. (48) are given by $\varphi^c_a=\delta^c_a$ with the corresponding eigenvalues satisfying $e^{1\uparrow}=e^{1\downarrow}\equiv e_1$ and $e^{2\uparrow}=e^{2\downarrow}\equiv e_2$. It then follows that $n^{1\uparrow}=n^{1\downarrow}\equiv n_1$, $n^{2\uparrow}=n^{2\downarrow}\equiv n_2$, $\Sigma_{1\uparrow,1\uparrow}=\Sigma_{1\downarrow,1\downarrow}\equiv\Sigma_1$, and $\Sigma_{2\uparrow,2\uparrow}=\Sigma_{2\downarrow,2\downarrow}\equiv\Sigma_2$. Inserting these formulas into Eq. (79) yields the self-energy equations $\Sigma_1=V_{12}n_2$ and $\Sigma_2=V_{12}n_1$.

At finite temperatures, the simultaneous solution of these self-energy equations and the band-filling constraint Eq. (53) must be performed numerically, but at $T=0$ the solution can be obtained analytically. In order to exhibit the zero-temperature solutions in a compact form, we define the noninteracting subband splitting in terms of the eigenvalues of Eq. (39): $\Delta^0_{\mathrm{SAS}}\equiv\epsilon_2-\epsilon_1$. The interaction renormalizes this splitting without modifying the identity of the underlying subbands. Applying the self-energy equations allows us to write this renormalized splitting as

$$\Delta^*_{\mathrm{SAS}}\equiv e_2-e_1=\Delta^0_{\mathrm{SAS}}+V_{12}(n_1-n_2). \tag{85}$$

If the chemical potential is measured from the bottom of the lower subband and $\mu<\Delta^*_{\mathrm{SAS}}$ then only the lower subband is occupied at zero temperature, and we shall refer to this state as the N_1 phase. Alternatively, if $\mu>\Delta^*_{\mathrm{SAS}}$, both subbands are occupied, and we shall refer to this as the N_2 phase. By solving the equations for Δ^*_{SAS} and the band filling constraint Eq. (53) simultaneously, we obtain

$$\Delta^*_{\mathrm{SAS}}=\begin{cases}\Delta^0_{\mathrm{SAS}}+\dfrac{1}{2}N_sV_{12} & (N_1 \text{ phase})\\ \dfrac{\Delta^0_{\mathrm{SAS}}}{1-N_0V_{12}} & (N_2 \text{ phase})\end{cases} \tag{86}$$

and

$$\mu=\begin{cases}\dfrac{N_s}{2N_0} & (N_1 \text{ phase})\\ \dfrac{N_s}{4N_0}+\dfrac{1}{2}\dfrac{\Delta^0_{\rm SAS}}{1-N_0V_{12}} & (N_2 \text{ phase}).\end{cases} \tag{87}$$

The crossover from N_1 to N_2 occurs when $\mu=\Delta^*_{\rm SAS}$ or $N_s/2N_0\Delta^0_{\rm SAS}=1/(1-N_0V_{12})$.

With the renormalized splitting $\Delta^*_{\rm SAS}$ and chemical potential μ computed, we are now in a position to study the collective intersubband spin-density excitations of this model to see if the excitonic instability occurs. The condition for these excitations obtained from Eq. (84) through the use of Eq. (83) is

$$1\pm{\rm Re}[\Pi^{12}(q,\omega)+\Pi^{21}(q,\omega)]V_{12}=0, \tag{88}$$

where the upper (lower) sign is for the spin (charge) density excitation, and we have dropped the spin indices since Π^{ab} does not depend on them in the normal state. At $\mathbf{q}=\mathbf{0}$ and $T=0$, an analytic solution for the frequency of the collective modes ω_0 is possible which is just the Ando result[27] with a renormalized subband splitting:

$$\omega_0^2=(\Delta^*_{\rm SAS})^2\mp 2V_{12}(n_1-n_2)\Delta^*_{\rm SAS}. \tag{89}$$

It is clear from this expression that the spin-density excitation (SDE) will soften completely when $\Delta^*_{\rm SAS}\leqslant 2V_{12}(n_1-n_2)$. At zero temperature, the relations derived in the preceding paragraphs can be used to show that the softening occurs in the N_1 phase when $N_sV_{12}/2\Delta^0_{\rm SAS}\geqslant 1$, and in the N_2 phase when $N_0V_{12}\geqslant\frac{1}{2}$. These boundaries are shown in Fig. 12 along with the line separating the N_1 and N_2 phases. The shaded area represents the region in which the spin-density excitation is soft at $q=0$ in this model. The phase corresponding to the soft mode occupies a large region of parameter space, and obtains at any density providing the interaction V_{12} is sufficiently strong.

At nonzero wave vector, Eq. (88) must be solved numerically. From the low-density N_1 phase, the results of this calculation are shown in Fig. 13 for increasing density at fixed interaction V_{12}. As illustrated by the figure, the $q=0$ spin-density excitation softens with increasing density and vanishes beyond a critical density which depends on the interaction strength V_{12}. At higher densities, the small-q solutions to Eq. (88) become imaginary, and the largest imaginary frequency—indicating the most unstable wave vector—continues to be at $q=0$. Thus, the transition from the low-density side is very clearly a $q=0$ instability, as is also seen in the TDLDA calculations.

The situation from the high-density N_2 side is more complicated. The dispersion curves for this case computed from Eq. (88) at fixed density and increasing interaction strength closely resemble those in Fig. 7. As the interaction strength V_{12} increases, the energy of the SDE's are reduced until the entire dispersion curve collapses along a range of wave vectors from $q=0$ to $k_{F1}-k_{F2}$, the difference of the Fermi wave vectors of the two subbands, at a critical V_{12}. The

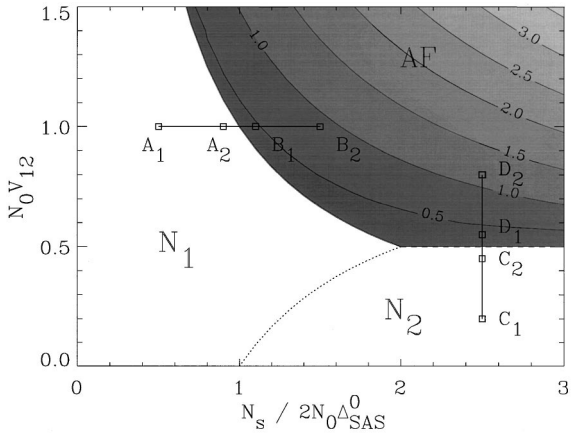

FIG. 12. Mean-field phase diagram of the antiferromagnetic sector of the point-contact model described in the text. The independent variables are the normalized intersubband interaction matrix element N_0V_{12} and the sheet density $N_s/2N_0\Delta^0_{\rm SAS}$, where $N_0=m^*/2\pi\hbar^2$ in the single-spin density of states and $\Delta^0_{\rm SAS}$ is the splitting between the lowest two subbands when $V_{12}=0$. The other interaction matrix elements $V_{11}=V_{22}=0$. The regions correspond to the normal (paramagnetic) phase with one subband occupied (N_1), the normal phase with both subbands occupied (N_2), and the antiferromagnetic phase (AF). Contours in the antiferromagnetic region of the phase diagram are the computed values of the critical temperature T_c for the antiferromagnetic transition in units of $\Delta^0_{\rm SAS}/k_B$. Observe that k_BT_c can be larger than $\Delta^0_{\rm SAS}$, indicating that the antiferromagnetic phase may persist to observable temperatures. The other labels in the figure identify points for future reference.

reason for this collapse is seen from Eq. (88) when one observes that, at $T=0$ in the N_2 phase,

$${\rm Re}[\Pi^{12}(q,\omega)+\Pi^{21}(q,\omega)]=-2N_0 \tag{90}$$

for $q<k_{F1}+k_{F2}$, indicating that if the energy of a SDE with one of these wave vectors vanishes, they all must vanish. At interaction strengths slightly larger than that required for a collapse, the solutions to Eq. (88) are imaginary in this range of wave vector, with the largest imaginary frequency occurring at $q=0$. These calculations suggest a $q=0$ transition from the high-density side, but the density-functional computations in Sec. III find a softening at the nonzero wave vector $q=k_{F1}-k_{F2}$. The discrepancy arises from the fact that the calculations in Sec. III include all the subband levels, whereas the model in this section contains only two. The inclusion of higher subbands, even if they are unoccupied, disrupt the cancellations leading to Eq. (90), and yield a q-dependent function which will select some wave vector. The consequences of a finite ordering vector will be discussed in Sec. VI, but are beyond the scope of our simple model. We nonetheless expect that many of the qualitative insights from our model will apply to more comprehensive theories.

One of the most important insights that can be gained by the study of the normal-state instability is a physical intuition about the nature of the ground state in the region of the phase diagram in which the SDE has softened. In structural phase transitions, a particular phonon softens, and the polarization

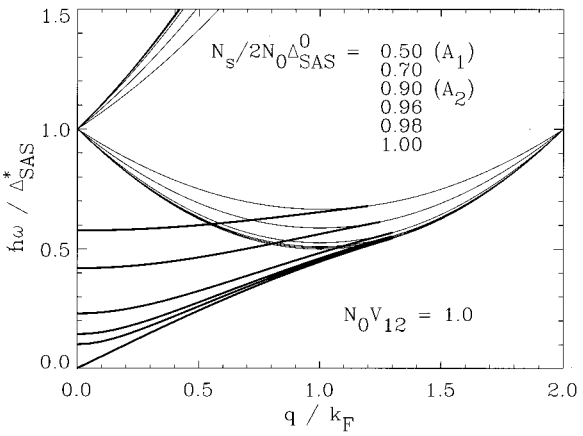

FIG. 13. Dispersion of the intersubband spin-density excitations (SDE's) as the sheet density N_s approaches the antiferromagnetic phase from the low-density, one-subband-occupied side computed in the antiferromagnetic sector of the point-contact interaction model discussed in the text with $N_0V_{12}=1.0$. The thick lines show the energy $\hbar\omega$ of the SDE's in units of the renormalized splitting of the lowest two subbands Δ^*_{SAS} as a function of wave vector q relative to the Fermi wave vector k_F. The thin lines show the boundaries of the particle-hole continuum, within which the collective excitations are damped. The sheet densities and corresponding points in the phase diagram of Fig. 12 are given in the figure. The transition to the antiferromagnetic phase occurs when the $q=0$ SDE's soften at $N_s/2N_0\Delta^0_{\mathrm{SAS}}=1.0$. A similar softening appears in Fig. 7, which shows the approach to the antiferromagnetic phase from the high-density side computed within the LDA.

of that phonon determines the structure. In the same way, the polarization of the soft spin-density excitation should reveal a great deal about the ground state. This polarization can be computed by means of Eqs. (74) and (75), which leads to a density response in the normal state given by

$$\langle\rho^{\mu}(\mathbf{R},t)\rangle\propto e^{i(\mathbf{q}\cdot\mathbf{r}-\omega t)}\xi_1(z)\xi_2(z)[\Pi^{12}(q,\omega)+\Pi^{21}(q,\omega)]\times(\hat{x}-i\hat{y}), \tag{91}$$

which is shown graphically in Fig. 14(a). Notice that the response occurs in the spin channel and has the character of a traveling wave transverse to the layering direction. Also observe that, since the wave function of the lowest subband $\xi_1(z)$ is even in z due to the assumed symmetry of the quantum-well structure, and the wave function of the next subband $\xi_2(z)$ is odd, the overall response odd in z. Thus the intersubband spin-density excitation corresponds to a spin-density wave in which the spin-density is antiferromagnetically correlated between the quantum wells.

With this interpretation, the nature of the excitonic instability becomes obvious: the softening of the $q=0$ SDE corresponds to the formation of antiferromagnetic order between the quantum wells with no modulation of the spin density within a well. A profile of the resulting spin density is presented in the inset of Fig. 15. Note that there are three degenerate SDE's in the normal phase which may be associated with spin polarizations along the three Cartesian directions. Although all three soften simultaneously, we expect that a particular spin direction will be selected by the system as in the ferromagnetic transition, but there is *a priori* no restriction of the direction of the spin polarization selected.

To summarize the results of the application of our simple model to the normal state, we find a softening of the intersubband spin-density excitations at $q=0$ for a wide range of model parameters. These collective excitations produce a spin-density modulation which is antiferromagnetically correlated between the wells. Thus the softening of the $q=0$ spin density modes indicate the formation of an antiferromagnetic phase in which the spins in both wells are polarized but in opposite directions. In the more realistic density-functional calculations of Sec. III, a $q\neq0$ instability was indicated, which would imply an additional intrawell modulation of the spin density (see Sec. VI). For simplicity, we focus on the $q=0$ phase.

C. Antiferromagnetic ground state and thermodynamics

With an understanding of the nature of the excitonic instability as an antiferromagnetic ordering, we are able to examine the ground state and its properties within our model. We first note that both spin rotation invariance and parity are broken in the antiferromagnetic state, so we are studying a genuine symmetry-breaking phase transition. The first task encountered in studying such a transition is to identify the order parameter. For concreteness, consider the antiferromagnetic phase with the spin density aligned along the $\hat{x}$ direction. From Eqs. (60) and (65), the only nonzero component of the spin density is then

$$\langle s^x(z)\rangle=\frac{\hbar}{2}\xi_{n_1}(z)\xi_{n_2}(z)\langle\rho_{n_1\uparrow,n_2\downarrow}(\mathbf{q}=\mathbf{0})\rangle. \tag{92}$$

Because the antiferromagnetism requires that $\langle s^x(z)\rangle$ be odd in z, only the terms which are off-diagonal in subband index are nonzero in this phase. Defining

$$\rho^{\mu}_{n_1n_2}=\sigma^{\mu}_{\sigma_1\sigma_2}\sum_{\mathbf{k}}\langle c^{\dagger}_{n_1\mathbf{k}\sigma_1}c_{n_2\mathbf{k}\sigma_2}\rangle, \tag{93}$$

and using Eq. (66), this implies that

$$\langle s^x(z)\rangle=\frac{\hbar}{2}\xi_{n_1}(z)\xi_{n_2}(z)\sum_{\mathbf{k}}[\langle c^{\dagger}_{1\mathbf{k}\uparrow}c_{2\mathbf{k}\downarrow}\rangle+\langle c^{\dagger}_{2\mathbf{k}\uparrow}c_{1\mathbf{k}\downarrow}\rangle \tag{94}$$

$$=\frac{\hbar}{2}\xi_{n_1}(z)\xi_{n_2}(z)[\rho^x_{12}+\rho^x_{21}]. \tag{95}$$

$\rho^x_{12}+\rho^x_{21}$ is finite in the antiferromagnetic phase and vanishes in the normal phase, so it is the order parameter of the phase transition. From the spin-rotational invariance of the system the direction in which the spin density can be polarized in the

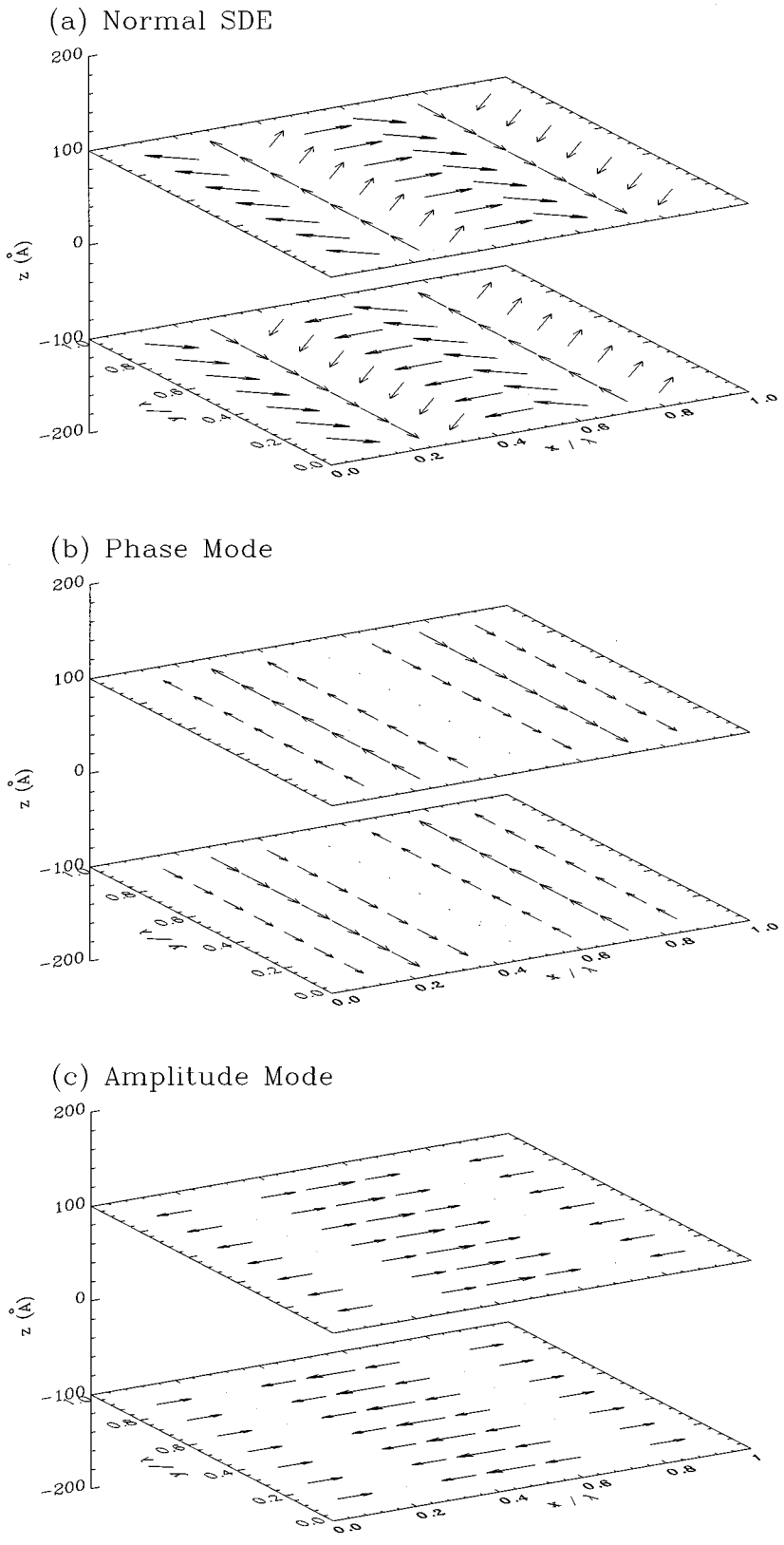

FIG. 14. Polarization of (a) an intersubband spin-density excitation in the normal phase and of the (b) phase (Nambu-Goldstone) and (c) amplitude modes in the antiferromagnetic phase with the spin density oriented along the $\hat{x}$ direction computed as described in the text. The configuration of the quantum wells is as in Fig. 1. The two planes are sections through this geometry normal to the layering direction and are located in the center of each well. The distances in these planes are measured in units of the wavelength of the collective excitation λ, whose propagation is in the $\hat{x}$ direction. The arrows show the direction and magnitude of the spin density modulation induced by the collective excitations. These modes have the form of a traveling wave, so the spin modulation at a different time is obtained by shifting these pictures along the $\hat{x}$ direction. Since the total spin density is the sum of the antiferromagnetic polarization and the modulations shown in (b) and (c), the identification of these modes with the phase and amplitude motions is apparent.

antiferromagnetic phase is arbitrary, so the general form of the order parameter is

$$N^i=\rho^i_{12}+\rho^i_{21}, \quad i=1,2,3. \tag{96}$$

With this identification, we can construct a form for the self-energy matrix which permits the off-diagonal expectation values we require, yet preserves the other symmetries of the system. This *ansatz* may be written[54]

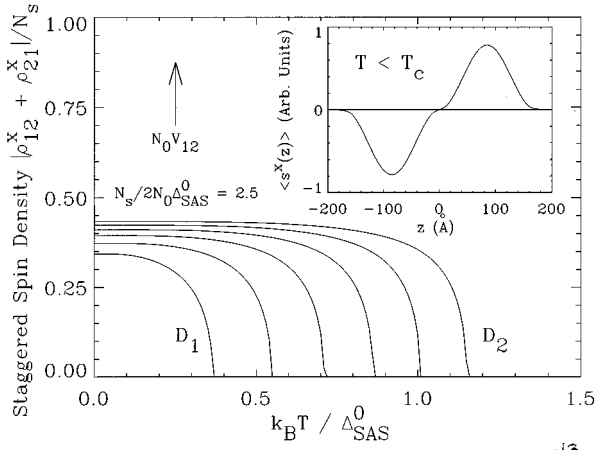

FIG. 15. Staggered spin density $(\rho^x_{12}+\rho^x_{21})$, which is the order parameter for the antiferromagnetic phase transition discussed in the text [cf. Eq. (96)], normalized by the electron sheet density N_s as a function of temperature T in units of the splitting between the two lowest subbands in the non-interacting limit $\Delta^0_{\rm SAS}$. The curves are computed for $N_s/2N_0\Delta^0_{\rm SAS}=2.5$ and N_0V_{12} = 0.55 to 0.80 in increments of 0.05; the lower and upper values correspond to points D_1 and D_2 in the phase diagram of Fig. 12. Inset: Expectation value of the spin density $\langle s^x(z)\rangle$ in real space as a function of the distance along the layering direction z for the double quantum well of Fig. 1 in the antiferromagnetic phase. Note that $\langle s^x(z)\rangle = 0$ in the paramagnetic phase.

$$\Sigma_{ab}=\begin{bmatrix}\Sigma_1 & 0 & 0 & \Sigma_{\rm od}\\ 0 & \Sigma_1 & \Sigma_{\rm od} & 0\\ 0 & \Sigma_{\rm od} & \Sigma_2 & 0\\ \Sigma_{\rm od} & 0 & 0 & \Sigma_2\end{bmatrix}. \tag{97}$$

Inserting this form into the eigenvalue equation Eq. (48) yields the eigenvectors

$$\varphi^c_a=\begin{bmatrix}u & 0 & 0 & -v\\ 0 & u & -v & 0\\ 0 & v & u & 0\\ v & 0 & 0 & u\end{bmatrix} \tag{98}$$

(columns correspond to the superscript) and eigenenergies $e^c=\{e^+,e^+,e^-,e^-\}$ [cf. Eq. (76)], where

$$\begin{pmatrix}u\\ v\end{pmatrix}=\left[\frac{1}{2}\left(1\mp\frac{\Delta^0_{\rm SAS}+\Sigma_2-\Sigma_1}{2D}\right)\right]^{1/2}, \tag{99}$$

$$e^{\pm}=\frac{\Delta^0_{\rm SAS}+\Sigma_2+\Sigma_1}{2}\pm D, \tag{100}$$

and

$$D=\left[\left(\frac{\Delta^0_{\rm SAS}+\Sigma_2-\Sigma_1}{2}\right)^2+\Sigma^2_{\rm od}\right]^{1/2}. \tag{101}$$

The eigenenergy spectrum indicates that the single-particle band structure in the antiferromagnetic phase consists of two sets of two degenerate parabolic subbands separated in energy by $\Delta_{+-}=e^+-e^-=2D$. This band structure is similar to that in the normal phases, but the wave functions of the interacting quasiparticles are considerably different: from Eq. (98), we see that these quasiparticles are linear combinations of electrons from the two noninteracting subbands.

The parameters in the eigenenergies and eigenvalues are determined from the self-consistency equations obtained by substituting the eigenvectors into reduced self-energy equation, Eq. (79). This procedure gives

$$\Sigma_1=V_{12}(n^-u^2+n^+v^2), \tag{102}$$

$$\Sigma_2=V_{12}(n^+u^2+n^-v^2), \tag{103}$$

and

$$\Sigma_{\rm od}=2V_{12}(n^--n^+)uv. \tag{104}$$

Using the definitions of u and v [Eq. (99)] and the band filling constraint

$$N_s=2(n^-+n^+), \tag{105}$$

these self-energy equations can be written

$$\Sigma_1+\Sigma_2=\frac{1}{2}V_{12}N_s, \tag{106}$$

$$\Delta^0_{\rm SAS}+\Sigma_2-\Sigma_1=\frac{\Delta^0_{\rm SAS}}{1-V_{12}(n^--n^+)/2D}, \tag{107}$$

and

$$\Sigma_{\rm od}=\frac{V_{12}(n^--n^+)}{D}\Sigma_{\rm od}. \tag{108}$$

In the antiferromagnetic phase, $\Sigma_{\rm od}\neq 0$, implying from Eq. (108) that $D=V_{12}(n^--n^+)$. Equation (107) then becomes $\Delta^0_{\rm SAS}+\Sigma_2-\Sigma_1=2\Delta^0_{\rm SAS}$ from which we obtain $D^2=(\Delta^0_{\rm SAS})^2+\Sigma^2_{\rm od}$ by Eq. (101). Comparing the two expressions for D yields

$$\Sigma_{\rm od}=[V^2_{12}(n^--n^+)^2-(\Delta^0_{\rm SAS})^2]^{1/2}. \tag{109}$$

The splitting between the interacting bands is

$$\Delta_{+-}=2D=2V_{12}(n^--n^+), \tag{110}$$

and the chemical potential is determined implicitly by Eq. (105).

At zero temperature, these equations can be easily solved. First, suppose $n^+=0$. Then Eqs. (105) and (109) imply that

$$\Sigma_{\rm od}=\left[\left(\frac{V_{12}N_s}{2}\right)^2-(\Delta^0_{\rm SAS})^2\right]^{1/2}, \tag{111}$$

Equation (110) becomes $\Delta_{+-}=V_{12}N_s$, and the band-filling constraint yields $N_s=2N_0\mu$. This solution is consistent if (1) $V_{12}N_s/2\Delta^0_{\rm SAS}\geqslant 1$ [Eq. (111)], and (2) $\mu\leqslant\Delta_{+-}$, which is equivalent to $N_0V_{12}\geqslant\frac{1}{2}$. These constraints are precisely those obtained in Sec. V B as the boundaries of the normal-state instability and are depicted in Fig. 12, demonstrating that $n^+=0$ over the entire range of the antiferromagnetic phase. Thus only the lowest ''-'' bands are occupied in this phase. From Eq. (111), we also observe that $\Sigma_{\rm od}$ rises from zero continuously along the boundary shared with the N_1 phase [cf. Fig. 12], indicating a second-order phase transition at

zero temperature. Along the boundary with the N_2 phase, however, $\Sigma_{\rm od}$ jumps discontinuously to a finite value, showing that this transition is *first*-order at $T=0$.

This interpretation is confirmed by a calculation of the energy change of the system across the transition, which also demonstrates the stability of the antiferromagnetic phase relative to the normal phases. From the relations

$$\frac{1}{A}\sum_{\mathbf{k}} f\left(\frac{\hbar^2k^2}{2m^*}-x\right)=N_0T\ \ln(e^{x/T}+1), \tag{112}$$

$$\mathrm{T}\vec{\rightarrow}0 N_0 x\,\theta(x) \tag{113}$$

and

$$\frac{1}{A}\sum_{\mathbf{k}} \frac{\hbar^2k^2}{2m^*}f\left(\frac{\hbar^2k^2}{2m^*}-x\right)\mathrm{T}\vec{\rightarrow}0 N_0\frac{x^2}{2}\,\theta(x), \tag{114}$$

and Eqs. (76), (42), (50), and (53), we can write the total energy [Eq. (57)] as

$$\frac{E}{A}=\frac{n^c}{2}(|\varphi_a^c|^2\epsilon_{n_a}+\mu). \tag{115}$$

Inserting the subband occupations, eigenvectors, and chemical potential obtained from the solution of the self-energy and band-filling equations at $T=0$, we find, for the N_1 phase,

$$\frac{E^{N_1}}{A}=\frac{N_s^2}{4N_0}, \tag{116}$$

for the N_2 phase,

$$\frac{E^{N_2}}{A}=\frac{N_s^2}{8N_0}(1+N_0V_{12})+\frac{\Delta_{\rm SAS}^0}{2}\left(N_s+\frac{N_0\Delta_{\rm SAS}^0}{1-N_0V_{12}}\right), \tag{117}$$

and, for the antiferromagnetic (AF) phase,

$$\frac{E^{\rm AF}}{A}=\frac{N_s^2}{4N_0}-\frac{1}{2N_0V_{12}}\left(\frac{N_sV_{12}}{2\Delta_{\rm SAS}^0}-1\right)^2. \tag{118}$$

We see immediately from Eqs. (116) and (118) that, in the range of parameter space in which both N_1 and AF solutions exist, $E^{\rm AF}<E^{N_1}$. In addition, the energy at the N_1-AF phase boundary [cf. Fig. 12] can be seen to be continuous and with continuous first derivatives. The second derivative is discontinuous at the phase boundary, however, showing that the phase transition is second order. Similarly, it can be shown that Eqs. (117) and (118) yield $E^{\rm AF}<E^{N_2}$ in the region of parameter space where both solutions exist, and that the *first* derivative of the energy difference at the phase boundary is discontinuous. Thus the antiferromagnetic phase is energetically stable with respect to the normal phases whenever the broken-symmetry solution exists, and the phase transition is second order from the N_1 phase and first order from the N_2 phase at zero temperature in mean-field theory.

At finite temperature, the self-energy equations in combination with the band-filling constraint must be solved numerically. The results of these computations can be used to obtain several quantities which characterize the antiferromagnetic phase: the transition temperature T_c and the temperature dependence of the order parameter $N^x=(\rho_{12}^x+\rho_{21}^x)$ and the specific heat c_V. The temperature at which the antiferromagnetic transition occurs is found by linearizing the self-energy equations in the off-diagonal self-energy $\Sigma_{\rm od}$. This procedure allows Eq. (108) to be written as

$$V_{12}(n^- - n^+)=\Delta_{\rm SAS}^0, \tag{119}$$

and also leads to the result $\Delta_{+-}=\Delta_{\rm SAS}^*$ for $\Delta_{\rm SAS}^*$ defined by Eq. (85). From these two expressions, we deduce that $\Delta_{+-}=2\Delta_{\rm SAS}$ at T_c. Thus the critical temperature is determined by the simultaneous solution of Eqs. (119) and (105) with the constraint $\Delta_{+-}=2\Delta_{\rm SAS}$. Using Eq. (112), we find that the T_c equation may be written, after some algebra, in the reduced variables $\beta_c=\Delta_{\rm SAS}^0/T_c$, $x=N_s/2N_0\Delta_{\rm SAS}^0$, and $y=N_0V_{12}$ as

$$2\beta_c=\ln\left[\frac{e^{\beta_c(xy+1)/2y}-1}{e^{\beta_c(xy-1)/2y}-1}\right]. \tag{120}$$

The reduced variables x and y are just the axes of the phase diagram in Fig. 12, in which the contours of constant $k_BT_c/\Delta_{\rm SAS}^0$ are also shown. We note that the critical temperature can be of the order of $\Delta_{\rm SAS}^0/k_B$, which may be on the order of 10 K for double quantum wells of the type shown in Fig. 1.

Below the transition temperature, the order parameter becomes finite, and we must solve the full nonlinear set of equations. To relate the self-energy parameters obtained in this way to the staggered spin density in Eq. (95), we first note that Eq. (51) can be used to show that

$$\sum_{\mathbf{k}}\langle c_{a\mathbf{k}}^\dagger c_{b\mathbf{k}}\rangle=\varphi_b^c n^c \varphi_a^{*c}. \tag{121}$$

Inserting this result into Eq. (95) and applying Eqs. (98) and (99), we find that the staggered magnetization

$$[\rho_{12}^x+\rho_{21}^x]=-2(n^- - n^+)\frac{\Sigma_{\rm od}}{\Delta_{+-}}. \tag{122}$$

At zero temperature, this expression reduces to

$$[\rho_{12}^x+\rho_{21}^x]=-N_s\left[1-\left(\frac{2\Delta_{\rm SAS}^0}{V_{12}N_s}\right)^2\right]^{1/2}. \tag{123}$$

Solving the $T>0$ self-energy and band-filling equations for a variety of interaction strengths, and substituting the results into Eq. (122), yields the curves in Fig. 15. We see that the staggered magnetization rises rapidly from zero below T_c, and saturates quickly to its $T=0$ value. This behavior is generally expected for an order parameter in mean-field theory.

Another quantity of theoretical and possibly experimental interest is the specific heat. The specific heat is proportional to the second derivative of the free energy with respect to temperature, so this quantity is discontinuous at either a first- or a second-order phase transition. This discontinuity is in principle measurable and would provide direct evidence of a thermodynamic phase transition occurring in these systems. Actually observing this discontinuity in semiconductor devices of the kind we are considering would be difficult, however, due to the low concentration of the relevant electrons. The specific heat is computed from Eq. (59) for a particular

temperature with the eigenenergies and chemical potential obtained from the self-consistency equations. Using Eq. (76) in Eq. (59), the specific heat per sample area may be written

$$c_V = N_0 T \sum_c \int_{-\beta(\mu-e^c)}^{+\infty} \frac{x e^x dx}{(e^x+1)^2} \left(x + \frac{d(\mu-e^c)}{dT} \right), \tag{124}$$

which at low temperature reduces to

$$c_V = \frac{\pi^2}{3} N_{\rm occ} N_0 T, \tag{125}$$

where $N_{\rm occ}$ is the number of occupied subbands: $N_{\rm occ}=2$ in the N_1 and AF phases and $N_{\rm occ}=4$ in the N_2 phase. Equation (125) is just the usual result obtained from a Sommerfeld expansion.[55]

Since we are aware of no calculations in the literature regarding the specific heat of a paramagnetic electron gas in a quantum-well structure, in Fig. 16(a) we present c_V for the noninteracting electron gas to use as a comparison for the interacting case. At low temperature, the curves naturally resolve themselves into two groups according to whether one or two subbands are occupied at $T=0$. This feature follows directly from Eq. (125) and is emphasized in the inset to Fig. 16(a). Observe that Eq. (125) is an inadequate description of c_V when T is larger than only a small fraction of the subband splitting $\Delta^0_{\rm SAS}$. The precise fraction is density dependent, as is whether the actual specific heat is smaller or larger than Eq. (125) predicts. The reason underlying this behavior is that, unlike the metallic case, the Fermi energy and the temperature are often comparable in these quantum-well structures, invalidating the Sommerfeld expansion. At higher temperatures, the form of the specific heat for both one- and two-subband-occupied ground states are similar, and have a magnitude at fixed temperature which increases monotonically with density. When the temperature becomes of the order of the energies of the higher subbands, this two-subband description breaks down. Of course, Eq. (124) may still be used to compute c_V at these temperatures, providing the higher subbands are included in this equation and the equation determining the chemical potential.

With the noninteracting specific heat as a baseline, we can now examine c_V in the interacting system in both the normal and antiferromagnetic phases. Figure 16(b) presents the specific heat as a function of temperature calculated for a fixed interaction strength. The different curves show the evolution of $c_V(T)$ as the density is increased from the single-subband-occupied N_1 phase into the antiferromagnetic phase. The specific heat in the N_1 phase is similar to the noninteracting plots in Fig. 16(a), exhibiting the low-temperature, linear-in-T behavior expected from Eq. (125) which crosses over at some density-dependent temperature $k_B T \ll \Delta^0_{\rm SAS}$ to an approximately constant value. As one enters the antiferromagnetic phase, one sees a discontinuity develop in c_V at T_c, which signals the phase transition. Unlike superconductivity,[47] there is no universal value for this discontinuity due to the large renormalizing effects of the temperature on the band-structure parameters. Above T_c, the curves resemble their normal-state counterparts, while, below T_c, the low-temperature result Eq. (125) seems to hold.

The latter behavior is not universal, however, as seen from Fig. 16(c). This figure shows the evolution of the specific-heat function at a fixed density and increasing interaction. The system is initially in the two-subband-occupied N_2 phase and becomes antiferromagnetic when $N_0 V_{12} > \frac{1}{2}$ (cf. Fig. 12). In the normal state, $c_V(T)$ has the shape expected from Fig. 16(a) with a low-temperature slope characteristic of having two subbands occupied [i.e., $N_{\rm occ}=4$ in Eq. (125)]. Increasing the interaction strength has only minor effects until the antiferromagnetic region of the phase diagram is reached, at which point c_V develops a discontinuity at T_c. At the same time, the slope of the low-temperature specific heat drops by a factor of 2 in accordance with Eq. (125) and the fact that only the lowest interacting bands are occupied in the antiferromagnetic state. Above T_c, the specific heat is qualitatively similar to the other normal-state curves. Below T_c, and in contrast to Fig. 16(b), $c_V \propto T$ at both low temperatures and temperatures near T_c but with different slopes. The slope near T_c is a function of the interaction strength and equals the low-temperature value for $N_0 V_{12}=1$; for $N_0 V_{12}>1$, the slope near T_c is actually less than the low-temperature slope.

D. Collective excitations

In addition to the ground-state and thermodynamic properties of the antiferromagnetic phase, it is also important to examine its collective excitations. The first indication of the antiferromagnetic phase transition is the disappearance of the intersubband spin-density excitations, and, on general theoretical grounds, one would like to know what replaces them in the broken-symmetry phase. Moreover, experimental studies of semiconductor heterostructures by inelastic light scattering can measure these excitations, and theory should provide some guidance about the expected signatures of the later phase. The latter point is particularly important in light of current searches for this phase.[56]

The basis for studying the collective modes in the antiferromagnetic phase is Eqs. (83) and (84) supplemented by the eigenvalues φ^c_a, eigenvectors e^c, and chemical potential determined as in Sec. V C. Because the wave functions of the interacting quasiparticles mix different subbands and spins, the bubble $\Pi^{(0)}_{ab,cd}(q)$ is no longer diagonal in these indices, and so Eq. (84) becomes a 16×16 matrix equation in subband and spin space. The remaining symmetries in the antiferromagnetic phase do not seem to be amenable to decomposing this matrix equation and arriving at an analytic solution, which forces us to adopt a numerical approach. We therefore obtain the interacting polarizability $\Pi_{ab,cd}(q)$ by direct numerical inversion of Eq. (84) at $T=0$, and identify the collective modes from the condition

$$\det[\,\delta_{ac}\delta_{bd} - \Pi^{(0)}_{ab,ef}(q)(V_{fe,cd} - V_{fd,ce})\,] = 0. \tag{126}$$

Since we are interested primarily in the intersubband spin-density modes, we will focus on the intersubband spin-flip polarizability

$$\Pi_{\rm inter}(q) \equiv f^{\rm ext}_{ab} \Pi_{ab,cd}(q) f^{\rm ext}_{cd}, \tag{127}$$

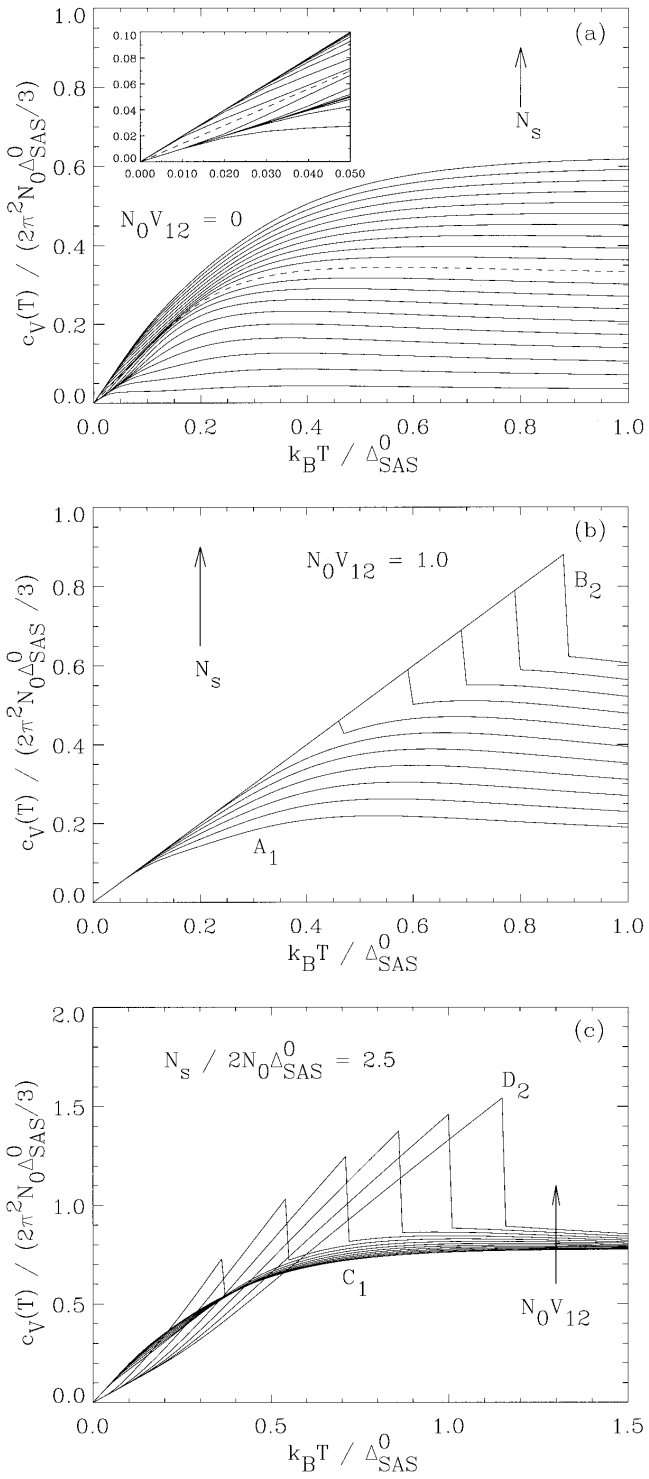

FIG. 16. Electronic specific heat at constant volume c_V is normalized by $2\pi^2 N_0 \Delta^0_{\rm SAS}/3$ as a function of the temperature T in units of $\Delta^0_{\rm SAS}/k_B$ for (a) $N_0V_{12}=0$ and $N_s/2N_0\Delta^0_{\rm SAS} = 0.1$ to 2.0 in increments of 0.1, (b) $N_0V_{12}=1$ and $N_s/2N_0\Delta^0_{\rm SAS} = 0.5$ to 1.5 in increments of 0.1 (i.e., along the line from A_1 to B_2 in Fig. 12), and (c) $N_s/2N_0\Delta^0_{\rm SAS} = 2.5$ and $N_0V_{12} = 0.2$ to 0.8 in increments of 0.05 (i.e., along the line from C_1 to D_2 in Fig. 12). The inset in (a) enlarges the low-temperature portion of the main figure in order to see the deviation from the analytic low-T expression, Eq. (125). Entrance into the antiferromagnetic phase is signaled by a discontinuity in the specific heat that is apparent in (b) and (c) but absent in (a).

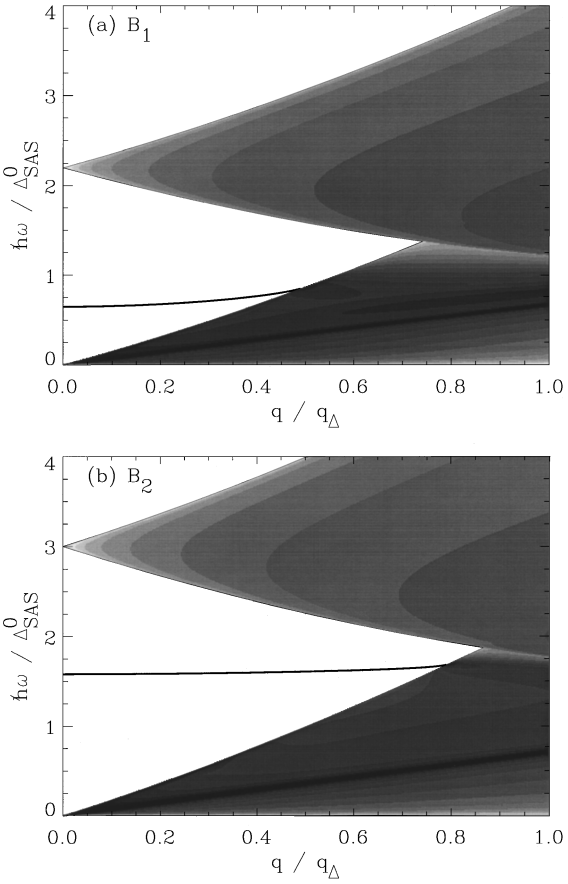

FIG. 17. Dispersion of the intersubband spin density collective modes in the antiferromagnetic phase at the points (a) B_1 and (b) B_2 of the phase diagram of Fig. 12, corresponding to $(N_s/2N_0\Delta^0_{\rm SAS}, N_0V_{12}) = (1.1,1.0)$ and (1.5,1.0), respectively. The thick lines are the energy $\hbar\omega$ in units of the non-interacting subband splitting Δ^0_{SAS} of the amplitude mode of the antiferromagnetic order parameter as a function of the wave vector q in units of $q^2_\Delta = m^*\Delta^0_{\rm SAS}/\hbar^2$. The shaded region is the particle-hole continuum, with darker shades representing larger spectral weight than lighter shades on a logarithmic intensity scale. The dark linear feature is the phase or Nambu-Goldstone mode of the order parameter. Note that this mode is damped by particle-hole excitations and that intrasubband excitations enter into the spectrum due to the mixing of the non-interacting wave functions in the symmetry-broken phase.

with $f^{\rm ext}_{ab}$ given by Eq. (75). Typical results for the spectral function of this polarizability in the antiferromagnetic phase, $-{\rm Im}\Pi_{\rm inter}(q)$, are shown in Fig. 17.

In analyzing these figures, it is useful to keep in mind the following facts about the band structure of the antiferromagnetic phase revealed by the analysis of Sec. V C: (1) the interacting band structure consists of two sets of two degenerate parabolic subbands separated by an energy Δ_{+-}, (2) only the lower set of interacting subbands are occupied, yielding a single Fermi wave vector k_F, and (3) the wave functions corresponding to the interacting bands are a mixture of the wave functions of the noninteracting subbands. Facts (1) and (2) indicate that the band structure is similar to that in the N_1 phase, so we expect to see a region of intersubband particle-hole excitations in the spectral function similar to those in Fig. 13. The kinematics of these excita-

tions require that their spectral weight start at $\hbar\omega=\Delta_{+-}$ at $q=0$, and spread within the boundaries given by

$$\frac{\hbar^2}{2m^*}(q-k_F)^2\leqslant\hbar\omega-\Delta_{+-}+\mu\leqslant\frac{\hbar^2}{2m^*}(q+k_F)^2 \tag{128}$$

for $q>0$ and μ measured from the bottom of the lowest interacting subband. In the normal phases, these intersubband excitations are cleanly separated from the intrasubband excitations by the projection in Eq. (127). In the antiferromagnetic state, however, fact (3) indicates that such a separation is impossible, leading to the additional low-frequency particle-hole continuum present in Fig. 17. Kinematics again show that this region is defined by $0<\omega\leqslant(\hbar^2/2m^*)\times(q+k_F)^2-\mu$ for $q<2k_F$. Although not shown in Fig. 17, at larger $q>2k_F$, the extent of this region of particle-hole excitations is defined by

$$\frac{\hbar^2}{2m^*}(q-k_F)^2-\mu\leqslant\omega\leqslant\frac{\hbar^2}{2m^*}(q+k_F)^2-\mu. \tag{129}$$

Within the particle-hole continuum, we find one striking feature at low frequencies which appears in Fig. 17 as a dark, linearly dispersing feature at low frequencies. Examining the solutions of Eq. (126),[57] we find that this feature is in fact a Landau-damped collective mode of the system. The polarization of this collective mode is extracted by returning to the full interacting polarizability $\Pi_{ab,cd}(q)$ and applying Eqs. (74) and (75) at the wave vectors and frequencies lying on the dispersion curve for this mode. A real-space representation of the resulting spin-density displacements is given in Fig. 14(b). To interpret these results, we first note that the antiferromagnetic phase for these calculations has its spin density oriented along the $\hat{x}$ direction. From Fig. 14(b), we see that the collective mode corresponds to a wave of antiferromagnetic spin displacements normal to this orientation, namely, in the $\hat{y}$ direction, traveling transverse to the layering direction of the quantum wells. The spin displacements are in opposite directions in different wells, so the net effect is a rotation of the total spin density in the xy plane that preserves the antiferromagnetic correlation of the spin density between the wells. Note that there is another collective mode degenerate with this one which corresponds to a rotation of the total spin density in the xz plane; this mode is projected out by our choice of $f_{ab}^{\rm ext}$ [Eq. (75)].

Outside of the particle-hole continuum, we can look for the undamped collective modes in the same way as in the preceding paragraph.[57] We find a single optical excitation whose dispersion is indicated by the thick black line in Fig. 17. The polarization of this mode is obtained from Eqs. (74) and (75), and is shown in Fig. 14(c). From this figure and our knowledge of the orientation of the spin density in the antiferromagnetic phase, we conclude that the optical mode corresponds to a modulation of the magnitude of the spin density which alters neither its direction in space nor the antiferromagnetic correlation between the wells. We note that, unlike the low-frequency mode, the optical mode becomes so strongly Landau damped once it enters the particle-hole continuum that it is no longer identifiable.

The two collective modes that appear in our calculations can be understood from general principles of phase transitions involving the breaking of a continuous symmetry.[58,49] In our case, the continuous symmetry is spin-rotation or $SU(2)$ invariance, and the extent to which it is broken is quantified by the staggered spin density **N** [Eq. 96)]. The collective modes in the broken-symmetry phase correspond to the modulation in space and time of either the direction or the magnitude of **N**, and are therefore called phase and amplitude modes, respectively. The polarization of the collective excitations discussed above unambiguously identify the two low-frequency, Landau-damped excitations as phase modes with orthogonal polarizations, and the optical excitation as the amplitude mode. This identification is strengthened by the dispersion of these excitations: the phase mode should have an energy which vanishes as $q\rightarrow0$, since ground states with different orientations of **N** are degenerate, whereas the amplitude mode should possess an excitation gap. These expectations are borne out in Fig. 17.

Further insight into these collective modes can be gained by following the evolution of the intersubband spin-density excitations as we change the parameters of our model and move from the normal to antiferromagnetic phases. We start in the single-subband-occupied N_1 phase at the point marked A_1 in Fig. 12. Increasing the density at fixed interaction, we move toward the antiferromagnetic phase (point A_2), causing the three degenerate intersubband spin-density excitations to soften as shown in Fig. 13. When the $q=0$ excitations vanish, the system enters the antiferromagnetic phase and the three intersubband SDE's turn into two degenerate phase modes and an amplitude mode as seen in Fig. 17(a). Increasing the density still further (to point B_2), the amplitude mode moves to higher frequencies while the phase mode is largely unchanged [Fig. 17(b)].

This behavior is typical of entry into the antiferromagnetic phase, and can be summarized by a plot of the $q=0$ intersubband excitation spectrum as a function of the model parameters, Fig. 18. In Fig. 18(a), we see the transition just described, in which the system is initially in the N_1 phase and the density is increased at fixed interaction strength. The collapse of the intersubband spin-density-excitation and the emergence of the amplitude mode is clearly seen. We also observe that both the splitting between the interacting subbands and the intersubband charge-density excitations are continuous and non-zero across the antiferromagnetic transition, but both have a discontinuity in their first derivatives.

The antiferromagnetic transition has a slightly different character when it proceeds from the two-subband-occupied N_2 side. Starting in the N_2 phase and increasing the interaction strength at fixed density, we see from Fig. 18(b) that the intersubband spin-density excitation softens as before, but the amplitude mode in the antiferromagnetic phase appears immediately thereafter at finite frequency. The interacting subband splitting and the intersubband charge-density excitation are also discontinuous across this phase boundary. These jumps are a consequence of the first-order nature of the $T=0$ antiferromagnetic transition from the N_2 side. Although finite temperatures will probably restore continuity to these curves, the large changes indicated may be experimentally observable and could provide strong evidence of the transition.

Whether the changes in the intersubband excitation spectrum we have discussed are observable in, for example, in-

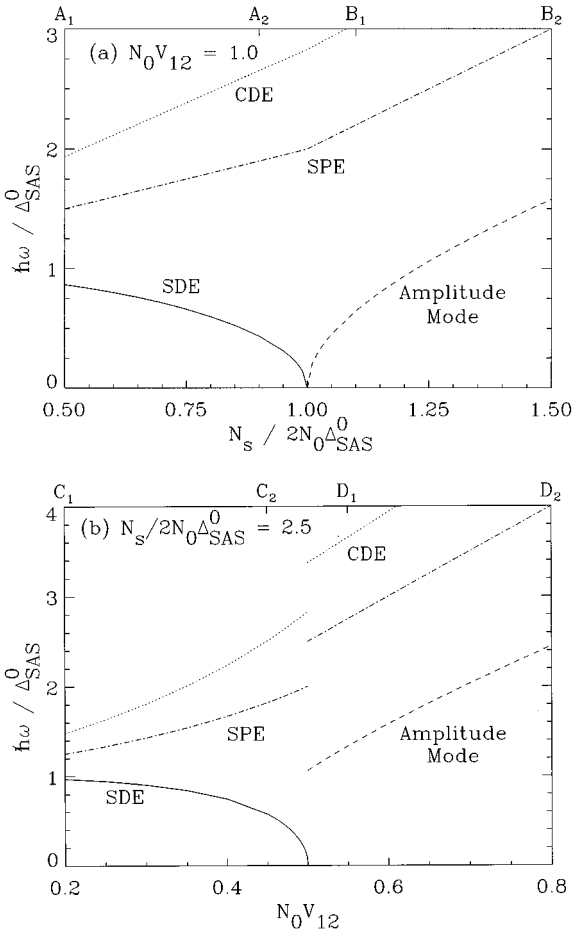

FIG. 18. Normalized energy $\hbar\omega/\Delta^0_{\rm SAS}$ of the $q=0$, $T=0$ collective excitations and interacting subband splitting for (a) a fixed interaction $N_0V_{12}=1.0$ and varying sheet density $N_s/2N_0\Delta^0_{\rm SAS}$ and (b) varying interaction N_0V_{12} and fixed sheet density $N_s/2N_0\Delta^0_{\rm SAS}=2.5$ in the antiferromagnetic sector of the point-contact model discussed in the text. Illustrated are the intersubband spin-density (SDE, solid lines) and charge density excitations (CDE, dotted lines), the renormalized subband splitting $\Delta^*_{\rm SAS}$ (SPE, dot-dashed lines), and the amplitude mode in the antiferromagnetic phase (dashed line). The top axes show the corresponding points in the phase diagram in Fig. 12. As seen in (b), the collective mode energies are discontinuous across the two-subband-occupied (N_2) to antiferromagnetic phase boundary at $T=0$, indicating a first-order transition.

elastic light-scattering experiments, depends to a great extent on the spectral weight associated with these features. As discussed in Ref. 25, peaks associated with the phase mode, the amplitude mode, and the intersubband particle-hole continuum should be visible in Raman spectra, but the response is dominated by the low-frequency phase mode. Most inelastic light-scattering measurements are done at small q and moderate frequencies, so the phase mode may be difficult to observe unless a concerted effort is made to look for it. Indeed, the signature of the antiferromagnetic phase in conventional light-scattering experiments may simply be the apparent absence of all intensity. We also note that the polarization of the scattered light relative to the antiferromagnetic ordering direction may affect the observed intensities of these modes. Since the ordering direction is arbitrary, this effect may result in a strong variation in the observed light-scattering spectra after temperature cycling above T_c or between different samples.

VI. DISCUSSION AND SUMMARY

In this paper, we studied the magnetic instabilities of semiconductor quantum wells within the local-density approximation to density-functional theory and a self-consistent Hartree-Fock theory. To create a consistent picture of the results of these calculations, one must realize that these two formalisms supply complementary information. The LDA computations are designed to be quantitatively reliable for the normal-state properties of these quantum-well structures. The self-consistent Hartree-Fock calculation, on the other hand, is only qualitatively reliable, but it is able to describe broken-symmetry phases that cannot be studied within the LDA. In particular, there is little point in trying to relate the parameters from the self-consistent Hartree-Fock calculation to the LDA results, because the former neglects such real-world effects as the distribution of the donor impurities which the latter includes. Hence the LDA calculations should indicate whether or not the transition occurs, and suggest the structures and densities at which to look for it, and the self-consistent Hartree-Fock calculations should provide information on the qualitative features of the resulting antiferromagnetic phase that can assist experimentalists in identifying it.

The only qualitative point about which the LDA and self-consistent Hartree-Fock calculations disagree is the ordering wave vector of the transition from the two-subband-occupied side of the phase diagram: the LDA yields $q_c=k_{F1}-k_{F2}$, while the self-consistent Hartree-Fock calculation gives $q_c=0$. As mentioned in Sec. V B, the discrepancy between the two formalisms can be traced back to the number of subbands included in the calculation and not to the form of the interaction, which is taken to be independent of wave vector in both cases. Since one expects a calculation including more subbands to be more accurate, it is reasonable to conclude that at least some part of the true phase diagram would have $q_c\neq 0$. That not all of the soft-SDE region of the phase diagram would have $q_c\neq 0$ is demonstrated by that fact that the one-subband-occupied SDE's unambiguously soften at $q_c=0$ in both the LDA and self-consistent Hartree-Fock theories. Since the latter theory focuses on interwell effects and neglects intrawell ones, its predictions regarding interwell properties such as the long-wave length intersubband spin-density excitations may be qualitatively valid even in the $q_c\neq 0$ phase. This phase would have a nontrivial spin-density modulation transverse to the quantum-well layering direction, but whether this modulation would be of the form of a simple spin-density wave or something akin to an antiferromagnetic Skyrmion lattice[59] in zero field cannot be determined from the present calculations. Future investigations exploring the $q_c\neq 0$ phase, and in particular the nature of the crossover between the $q_c=0$ and $q_c\neq 0$ phases, could in principle be performed within a generalization of the self-consistent Hartree-Fock formalism discussed in this paper.

Our calculations have focused on the physics along the layering direction, and it is reasonable to ask to what extent exchange and correlation normal to the layering direction

have been included. In addressing this point, it is useful to discuss the local-density approximation (LDA) and self-consistent Hartree-Fock calculations separately. In the LDA, the effects of exchange and correlation are approximated by a functional of the local electron density. The form of this functional is deduced from Monte Carlo calculations for a free-electron gas in either two or three dimensions. If the ground state of the quantum-well system is translationally invariant along the plane of the wells, then the local electron density depends only on the coordinate normal to the plane of the wells, z, leading to Eq. (1). Although an explicit function only of z, the effective potential implicitly includes the effects of exchange and correlation along the plane of the wells through our choice of the exchange-correlation potential [Eq. (31)]. The form of the interaction then allows us to separate the electronic wave function into a confined component along the layering direction and a plane-wave component normal to it [cf. Eqs. (3) and (40)]. This approach is the conventional one and underlies almost all calculations of the physical properties of metal-organic semiconductor field-effect transistors and GaAs heterostructures.[60]

This approach fails if either the translational invariance is broken or the LDA is no longer a good approximation. The loss of translational invariance occurs in the Wigner solid or in the $q_c \neq 0$ phase discussed above; the LDA can only examine the boundaries of these phases but not their properties. The range of validity of the LDA as a whole is somewhat trickier to ascertain, but its use can be justified by the remarkable agreement between its predictions and experiment in both fully three-dimensional and low-dimensional confined quantum systems.[19,23,22,61] We may therefore conclude that our LDA calculations contain an appropriate amount of in-plane exchange and correlation effects. Indeed, if that were not the case, the LSDA would see no ferromagnetic transition at all.

The main effect of in-plane exchange-correlation corrections, as long as there is no exchange-correlation-induced quantum phase transition or planar symmetry breaking of the type discussed above (e.g., Wigner crystallization or ferromagnetism), is to introduce many-body Fermi-liquid renormalization of the various one-electron parameters such as the effective mass and band gap which enter into the LDA calculations. Such two-dimensional renormalization effects in GaAs quantum wells have been extensively studied in the literature,[62] and the quantitative corrections are usually not very large. The LDA calculations should be presumed to be carried out using effective parameters (e.g., effective mass) which already incorporate these two-dimensional renormalization effects. Thus the LDA should be considered an effective theory for describing the normal-state intersubband electronic properties. In general, LDA-type calculations have historically been extremely successful in quantitatively determining the intersubband collective mode energies in GaAs quantum wells (see Ref. 24, for example). A full calculation of the quantum phase transition predicted and studied in our paper which includes the complete effects of the Coulomb interaction both in the plane and perpendicular to it is obviously well beyond the scope of current-day computational resources, and is quite unnecessary for the reasons discussed above.

The self-consistent Hartree-Fock calculations in this paper also include the approximate effects of in-plane exchange. We take the screened Coulomb interaction which enters the self-energy equations to be a δ function in three-dimensional space. Calculating the properties of our double-quantum-well system with this model interaction automatically involves exchange effects both along and normal to the layering direction, although this fact may not be apparent from the simple wave-vector dependence of this interaction when expressed in terms of the basis of Eq. (40). Other workers[63] solve essentially the same equations in the normal state, but choose different form for the screened Coulomb interaction. As argued above, our admittedly crude approximation to the interaction should nonetheless allow the study of the qualitative features of the antiferromagnetic phase whose boundary is quantitatively predicted by the LDA.

With these comments in mind, let us summarize the primary results of this work. We have presented a TDLDA calculation which shows that the intersubband spin-density excitations (SDE's) in certain coupled double- and wide single-quantum-well structures soften completely in a range of densities around the point where the second subband begins to populate (10^{10}–10^{11} cm^{-2}) and in the absence of an external magnetic field. Based on these calculations, we constructed a phase diagram indicating the structures likely to exhibit this instability. We also computed the excitation spectrum measurable by inelastic light scattering near the instability in order to illustrate how the SDE softening would appear in these experiments. Since the TDLDA yields both spin- and charge-density excitation spectra which are in very good quantitative agreement with experiment,[15,16,22] the softening of the spin-density excitations should be observable in the appropriate range of densities.

In trying to understand this instability, we have explored the possibility of ferromagnetic transitions in double- and single-quantum-well structures by including the spin degree of freedom in a density-functional calculation within the LSDA. We find that a ferromagnetic transition occurs in the double-quantum-well structures which exhibit SDE softening, but that the transition occurs at much lower ($\sim 10^9$ cm^{-2}) densities, implying that the SDE softening cannot be associated with ferromagnetism. In square single quantum wells, our computations provide evidence of a spin-polarized phase of the electron gas which lies between the Wigner crystal and normal phases. The critical density for this transition decreases with increasing well width, demonstrating that exchange-correlation effects are stronger in lower dimensions, as expected from a simple Hartree-Fock analysis.

Having failed to identify the SDE-softened phase within density-functional theory, we turned to a simple model of coupled double quantum wells which we treated within self-consistent Hartree-Fock theory. This model is able to reproduce the SDE softening in its normal state, and the polarization of the soft mode indicates that the softening signals the onset of antiferromagnetic order in the spin density between the wells. Extending our calculations into the antiferromagnetic phase, we found that this phase exists and is stable over a wide range of parameters, and that the mean-field transition temperature can be of the same order as the symmetric-antisymmetric splitting. In addition, we found that the transition to this phase at zero temperature is second order from the single-subband-occupied side of the phase diagram, but

first order from the two-subband-occupied side. Due to the absence of an energy gap in the single-particle spectrum, we do not expect strong anomalies in the transport properties to accompany the transition; however, our calculations of the electronic specific heat show that, if this quantity is measurable, it will show a characteristic discontinuity at the transition temperature. A means of searching for the transition which is more likely to succeed is the measurement of the collective spin-density excitations through inelastic light scattering. By computing the spectrum of these excitations in the antiferromagnetic phase, we identify a Landau-damped phase mode of the order parameter and a true optical collective excitation corresponding to the amplitude mode. The spectral weight associated with the phase mode is large, suggesting that inelastic light-scattering experiments should look at low frequencies for this characteristic excitation of the antiferromagnetic phase.

In closing, we note that at least one experimental group has investigated the possibility of an antiferromagnetic phase transition of the type we describe by performing resonant inelastic light-scattering measurements on double-quantum-well structures.[56] The results, however, have been mixed. In zero field, the complete softening of the spin-density excitation does not seem to appear in the electron density regime ($\approx 5\times 10^{10}$ cm^{-2}) predicted by the TDLDA theory. It is possible, of course, that impurity-scattering-induced broadening effects make it impossible to observe the complete softening of the spin-density excitation. Alternatively, the TDLDA theory may overestimate the density range in which the transition occurs, implying that the actual antiferromagnetic instability may take place at lower electron densities. A third possibility is that the TDLDA approach may simply be inadequate for studying semiconductor quantum wells at the low densities involved.

More promising are the experimental results in small but finite magnetic fields along the layering direction, which do indicate a softening of the intersubband spin-density excitations at the filling factors $\nu=2$ and 6.[56] The general observation of the softening of the intersubband spin-density excitations in the presence of a magnetic field[56] is qualitatively consistent with the prediction of our zero-field theory, since a magnetic field weak enough so that the system in not completely spin-polarized enhances the effects of the interaction by reducing the kinetic energy through Landau quantization. Thus, the magnetic field naturally enhances the potential for the type of spin instabilities discussed in this paper to appear. Moreover, the basic Hartree-Fock theory underlying the description of the resulting broken-symmetry states do not change, although the effects of Landau-level quantization should be included. Such a generalization of the self-consistent Hartree-Fock approach is straightforward, and is left for future work.

ACKNOWLEDGMENTS

The authors would like to thank R. Decca and P. B. Littlewood for useful discussions. This work was supported by the U.S. Office of Naval Research.

*Present address: Division of Applied Sciences, Harvard University, Cambridge, MA 02138.

†Present address: Institut für Theoretische Physik, J. W. Goethe Universität Frankfurt, Robert-Mayer-Str. 8, D-60 054 Frankfurt a.M., Germany.

[1] D. C. Tsui, H. L. Störmer, and A. C. Gossard, Phys. Rev. Lett. **48**, 1559 (1982).

[2] R. B. Laughlin, Phys. Rev. Lett. **50**, 1395 (1983).

[3] H. A. Fertig, Phys. Rev. B **40**, 1087 (1989); A. H. MacDonald, P. M. Platzman, and G. S. Boebinger, Phys. Rev. Lett. **65**, 775 (1990); L. Brey, *ibid.*, **65**, 903 (1990); X. Chen and J. J. Quinn, *ibid.* **67**, 895 (1991); S. He, X. C. Xie, S. Das Sarma, and F. C. Zhang, Phys. Rev. B **43**, 9339 (1991).

[4] G. S. Boebinger, H. W. Jiang, L. N. Pfeiffer, and K. W. West, Phys. Rev. Lett. **64**, 1793 (1990).

[5] Y. W. Suen, L. W. Engel, M. B. Santos, M. Shayegan, and D. C. Tsui, Phys. Rev. Lett. **68**, 1379 (1992); J. P. Eisenstein, G. S. Boebinger, L. N. Pfeiffer, K. W. West, and S. He, *ibid.*, **68**, 1383 (1992).

[6] R. J. Price, P. M. Platzman, and Song He, Phys. Rev. Lett. **70**, 339 (1993).

[7] S. He, S. Das Sarma, and X. C. Xie, Phys. Rev. B **47**, 4411 (1993), and references therein.

[8] B. I. Halperin, P. A. Lee, and N. Read, Phys. Rev. B **47**, 7312 (1993).

[9] E. P. Wigner, Phys. Rev. **46**, 1002 (1934); Trans. Faraday Soc. **34**, 678 (1938).

[10] C. C. Grimes and G. Adams, Phys. Rev. Lett. **42**, 795 (1979).

[11] S. F. Edwards and A. J. Hillel, J. Phys. C **1**, 61 (1968); A. W. Overhauser, Phys. Rev. Lett. **3**, 414 (1959); **4**, 462 (1960); Phys. Rev. **128**, 1437 (1962).

[12] F. Bloch, Z. Phys. **57**, 549 (1929).

[13] A. H. MacDonald, Phys. Rev. B **37**, 4792 (1988).

[14] C. M. Varma, A. I. Larkin, and E. Abrahams, Phys. Rev. B **49**, 13 999 (1994).

[15] A. Pinczuk, S. Schmitt-Rink, G. Danan, J. P. Valladares, L. N. Pfeiffer, and K. W. West, Phys. Rev. Lett. **63**, 1633 (1989); S. L. Chuang, M. S. C. Luo, S. Schmitt-Rink, and A. Pinczuk, Phys. Rev. B **46**, 1897 (1992).

[16] D. Gammon, B. V. Shanabrook, J. C. Ryan, and D. S. Katzer, Phys. Rev. B **41**, 12 311 (1990); D. Gammon, B. V. Shanabrook, J. C. Ryan, D. S. Katzer, and M. J. Yang, Phys. Rev. Lett. **68**, 1884 (1992).

[17] P. P. Ruden and Z. Wu, Appl. Phys. Lett. **59**, 2165 (1991).

[18] L. Świerkowski, D. Neilson, and J. Szymański, Phys. Rev. Lett. **67**, 240 (1991); D. Neilson, L. Świerkowski, J. Szymański, and L. Liu, *ibid.* **71**, 4035 (1993).

[19] S. Das Sarma and I. K. Marmorkos, Phys. Rev. B **47**, 16 343 (1993); I. K. Marmorkos and S. Das Sarma, *ibid.* **48**, 1544 (1993); and references therein.

[20] Y. Katayama, D. C. Tsui, H. C. Manoharan, and M. Shayegan, Surf. Sci. **305**, 405 (1994); Phys. Rev. B **52**, 14 817 (1995); and X. Ying, S. R. Parihar, H. C. Manoharan, and M. Shayegan, *ibid.* **52**, 11 611 (1995).

[21] R. Decca, A. Pinczuk, S. Das Sarma, B. S. Dennis, L. N. Pfeiffer, and K. W. West, Phys. Rev. Lett. **72**, 1506 (1994).

[22] P. I. Tamborenea and S. Das Sarma, Phys. Rev. B **49**, 16 821 (1994).

[23] S. Ernst, A. R. Goñi, K. Syassen, and K. Eberl, Phys. Rev. Lett. **72**, 4029 (1994).

[24] S. Das Sarma and P. I. Tamborenea, Phys. Rev. Lett. **73**, 1971 (1994).

[25] R. J. Radtke and S. Das Sarma, Solid State Commun. **96**, 215 (1995); **98**, 771 (1996).
[26] As we shall see later, it is actually somewhat misleading to think about the spin-density-excitation condensate as a sea of bound electron-hole pairs from different subbands.
[27] T. Ando, Surf. Sci. **58**, 128 (1976); Phys. Rev. B **13**, 3468 (1976).
[28] T. Ando, J. Phys. Soc. Jpn. **51**, 3893 (1982); S. Katayama and T. Ando, *ibid.* **54**, 1615 (1985).
[29] A. Pinczuk and G. Abstreiter, in *Light Scattering in Solids V*, edited by M. Cardona and G. Guntherodt (Springer-Verlag, Berlin, 1989).
[30] S. Das Sarma, in *Light Scattering in Semiconductor Structures and Superlattices*, edited by D. J. Lockwood and J. F. Young (Plenum, New York, 1991).
[31] P. Hohenberg and W. Kohn, Phys. Rev. **136**, B864 (1964).
[32] W. Kohn and L. J. Sham, Phys. Rev. **140**, A1133 (1965).
[33] F. Stern and S. Das Sarma, Phys. Rev. B **30**, 840 (1984).
[34] D. M. Ceperley and B. J. Alder, Phys. Rev. Lett. **45**, 566 (1980); J. Perdew and A. Zunger, Phys. Rev. B **23**, 5048 (1981).
[35] D. C. Hamilton and A. L. McWhorther, in *Light Scattering Spectra in Solids*, edited by G. B. Wright (Springer-Verlag, Berlin, 1969), p. 309.
[36] A. L. Fetter and J. D. Walecka, *Quantum Theory of Many-Particle Systems* (McGraw-Hill, New York, 1971).
[37] S. Das Sarma, in *Light Scattering in Semiconductor Structures and Superlattices* (Ref. 30), and references therein.
[38] J. K. Jain and S. Das Sarma, Phys. Rev. B **36**, 5949 (1987).
[39] U. von Barth and L. Hedin, J. Phys. C **5**, 1629 (1972).
[40] M. M. Pant and A. K. Rajagopal, Solid State Commun. **10**, 1157 (1972).
[41] R. M. Dreizler and E. K. U. Gross, *Density Functional Theory* (Springer-Verlag, Berlin, 1990).
[42] A .K. Rajagopal and J. C. Kimball, Phys. Rev. B **15**, 2819 (1977).
[43] D. M. Ceperley (private communication).
[44] B. Tanatar and D. M. Ceperley, Phys. Rev. B **39**, 5005 (1989).
[45] S. Das Sarma and B. Vinter, Phys. Rev. B **26**, 960 (1982); **28**, 3639 (1983).
[46] C. E. Hembree, B. A. Mason, J. T. Kwiatkowski, J. Furneaux, and J. A. Slinkman, Phys. Rev. B **48**, 9162 (1993).
[47] J. R. Schrieffer, *Theory of Superconductivity* (Addison-Wesley, New York, 1964).
[48] G. D. Mahan, *Many-Particle Physics* (Plenum, New York, 1981).
[49] See, for example, D. Forster, *Hydrodynamic Fluctuations, Broken Symmetry, and Correlation Functions* (Addison-Wesley, New York, 1975).
[50] G. Baym and L. P. Kadanoff, Phys. Rev. **124**, 287 (1961); G. Baym, *ibid.* **127**, 1391 (1962).
[51] We can obtain a crude estimate of the upper limit to the transition temperature T_c by putting $k_B T_c \approx \triangle_{\rm SAS}$, which makes the TDLDA calculations meaningful only for $T \ll T_c \approx \triangle_{\rm SAS}/k_B$. For $T \approx$ 1–4 K, this restricts $d_B \leqslant$ 45–50 Å.
[52] O. Gunnarsson and B. I. Lundqvist, Phys. Rev. B **13**, 4274 (1976).
[53] For a review, see B. I. Halperin and T. M. Rice, in *Solid State Physics*, Vol. 21, edited by F. Seitz, D. Turnbull, and H. Ehrenreich (Academic, New York, 1968), p. 115.
[54] This *ansatz* is confirmed by numerical solution of the complete self-energy equations with the band-filling constraint.
[55] N. W. Ashcroft and N. D. Mermin, *Solid State Physics* (Saunders College, Philadelphia, 1976), Chap. 1.
[56] A. S. Plaut, A. Pinczuk, B. S. Dennis, J. P. Eisenstein, L. N. Pfeiffer, and K. W. West, Surf. Sci. **361/362**, 158 (1996); A. S. Plaut, Bull. Am. Phys. Soc. **41**, 590 (1996); and (private communication).
[57] For technical reasons, it actually is more convenient to find the collective modes in the intersubband spin-density channel by locating the points where $1/{\rm Re}\Pi_{\rm inter}(q)=0$ rather than solving Eq. (126) directly. The two methods yield identical results for the intersubband SDE modes.
[58] Y. Nambu and G. Jona-Lasinio, Phys. Rev. **122**, 345 (1961); J. Goldstone, Nuovo Cimento **19**, 154 (1961).
[59] L. Brey, H. A. Fertig, R. Coté, and A. H. MacDonald, Phys. Rev. Lett. **75**, 2562 (1995).
[60] T. Ando, A. B. Fowler, and F. Stern, Rev. Mod. Phys. **54**, 437 (1981).
[61] However, some problems involving *interband* excitons may require a more sophisticated variational treatment. See G. Bastard, E. E. Mendez, L. L. Chang, and L. Esaki, Phys. Rev. B **26**, 1974 (1982); D. A. B. Miller, D. S. Chemla, T. C. Damen, A. C. Gossard, W. Wiegmann, T. H. Wood, and C. A. Burrus, *ibid.* **32**, 1043 (1985); J. W. Wu and A. V. Nurmikko, *ibid.* **36**, 4902 (1987); Y. P. Feng and H. N. Spector, *ibid.* **48**, 1963 (1993); Y. Shinozuka and M. Matsuura, *ibid.* **28**, 4878 (1983); **29**, 3717 (1984).
[62] R. Jalabert and S. Das Sarma, Phys. Rev. B **40**, 9723 (1989); S. Das Sarma, R. Jalabert, and S. R. E. Yang, *ibid.* **41**, 8288 (1990); I. K. Marmorkos and S. Das Sarma, *ibid.* **44**, 3451 (1991).
[63] S. Schmitt-Rink, C. Ell, S. W. Koch, and H. Haug, Solid State Commun. **52**, 123 (1984); S. Schmitt-Rink and C. Ell, J. Lumin. **30**, 585 (1985).